PHYSIOLOGY

Bcl-xL overexpression in T cells preserves muscle mitochondrial structure and function and prevents frailty in old mice

Cristina Mas-Bargues[1,2]†, Aurora Román-Domínguez[1]†, Jorge Sanz-Ros[1]‡, Nekane Romero-García[1]§, Javier Huete-Acevedo[1], Mar Dromant[1], Ana María Cuervo[2], Consuelo Borrás[1]*, José Viña[1]

Our previous transcriptomic analysis revealed an up-regulation of the antiapoptotic protein B cell lymphoma-extra large (Bcl-xL) in centenarians relative to octogenarians or younger cohorts. In this study, we used Bcl-xL–overexpressing mice to assess its impact on successful aging. Our findings indicate that Bcl-xL overexpression modifies T cell subsets and improves their metabolism, apoptosis resistance, macroautophagy, and cytokine production during aging. This more resilient immune system reduces inflammation and preserves mitochondrial integrity and function in muscle tissue, thereby retarding the onset of frailty. These results underscore the important contribution of Bcl-xL to healthy aging, a phenomenon that is conserved across mammalian species.

INTRODUCTION

In the pursuit of unraveling the secrets behind healthy aging and longevity, centenarians stand as remarkable icons of enduring vitality. These individuals, having reached the rare milestone of living beyond 100 years, offer invaluable insights into the intricate interplay of genetics, lifestyle, and environmental factors that contribute to a prolonged and healthy life. Centenarians are a model of successful aging because they seem to avoid the age-related organ deterioration of tissue structure and function, which markedly increases the risk of chronic pathologies (*1*).

The recent conceptualization of geroscience envisages that a few selected and intertwined biological processes represent the critical pillars of aging and age-related diseases (*2*). Immunosenescence and inflammaging stand out as important among these processes.

The immune system exhibits remarkable changes during aging that affect both natural and acquired immunity and play a critical role in most chronic diseases in the elderly (*3*). Our previous studies reported that centenarians' blood displays a unique transcriptome that more closely resembles that of young individuals than old ones. Subnetwork analysis of the 1721 mRNAs differentially expressed in peripheral blood mononuclear cells from centenarians, septuagenarians, and young people converged in the B cell lymphoma-extra large (Bcl-xL) gene, which was overexpressed in centenarians (*4*). Its main role is to regulate the outer mitochondrial membrane integrity, thereby preventing cytochrome c release and avoiding apoptosis (*5*). Thus, Bcl-xL enables a fine-tuned regulation of intrinsic apoptosis, as well as modulates mitochondrial bioenergetics and oxidative stress, which helps, among others, to prevent the accumulation of senescent immune cells, thereby maintaining a fully functional immune system (*6*).

This is important because immunosenescence has been considered a major cause of inflammaging, a low-grade sterile chronic inflammation (*7*). Inflammaging is involved in the etiology and progression of age-related diseases and has been associated with impaired muscle regeneration and a progressive decline of muscle mass and strength, ultimately leading to sarcopenia (*8*). Sarcopenia is the loss of muscle mass and function in the elderly that reduces mobility, diminishes the quality of life, and can lead to fall-related injuries, which require costly hospitalization and extended rehabilitation. Sarcopenia is linked to the physical aspects of frailty, a multisystem impairment associated with increased vulnerability to stressors (*9*).

Aging and muscle disuse are associated with reductions in muscle mass and strength that are in part attributable to dysregulation of the mitochondrial network and impaired mitochondrial function. Mitochondria are implicated in a spectrum of pivotal cellular functions within the skeletal muscle that are essential for sustaining normal muscular operation, such as adenosine 5′-triphosphate (ATP) production and protein homeostasis (*10*). It has recently been suggested that chronic inflammation promotes mitochondrial dysfunction through modulations in apoptotic induction and the suppression of mitochondrial biogenesis (*11*). Changes in the different T cell subset ratios and an altered cytokine expression during aging may contribute to an imbalance between the pro-inflammatory and anti-inflammatory immune responses, thereby modulating mitochondrial function and altering the regenerative capacity of skeletal muscle cells.

To understand the direct consequences of increased expression of Bcl-xL, we used the transgenic mouse model that overexpresses human Bcl-xL in all T cell subsets. Bcl-xL expression decreases in T cells during aging, but B cells retain inducible expression of Bcl-xL with age (*12*–*14*). Thus, the aging effect on Bcl-xL appears more pronounced in T cells, indicating a specific vulnerability in these cells' survival pathways as individuals age. In this study, using this model, we have found a protective role of Bcl-xL against a variety of apoptotic stimuli in a similar way to centenarians. It is worth noting that this mouse model has been characterized from an aging point of

[1]Freshage Research Group, Department of Physiology, Faculty of Medicine, University of Valencia, Centro de Investigación Biomédica en Red Fragilidad y Envejecimiento Saludable-Instituto de Salud Carlos III (CIBERFES-ISCIII), INCLIVA, 46010 Valencia, Spain. [2]Department of Developmental and Molecular Biology, Institute for Aging Research, Albert Einstein College of Medicine, Bronx, NY 10461, USA.
*Corresponding author. Email: consuelo.borras@uv.es
†These authors contributed equally to this work.
‡Present address: Department of Pathology, Stanford University, Stanford, CA 94305, USA.
§Present address: Department of Anesthesiology and Surgical Trauma Intensive Care, Hospital Clinic Universitari de Valencia, University of Valencia, 46010 Valencia, Spain.

view. We demonstrate that overexpression of Bcl-xL in T cells promotes T regulatory cell infiltration in skeletal muscle and maintains the muscle mitochondrial structure and function, thereby preventing frailty in old age.

RESULTS

Bcl-xL overexpression does not alter T cell subsets but modulates their metabolism, apoptosis resistance, and cytokine secretion pattern during aging

In our isolation procedure of T cells from spleens, we observed a substantial increase in the T cell yield from Bcl-xL–overexpressing animals compared with controls at young and adult ages (Fig. 1, A and B). This Bcl-xL overexpression does not alter $CD3^+$hi and $CD3^+$lo during aging, as no differences were observed when comparing wild-type and transgenic mice (Fig. 1C). We measured the dynamics of T cell subsets in our mouse models across aging. We specifically evaluated the proportions of $CD4^+$ T helper cells, $CD8^+$ cytotoxic T cells, and their respective naïve, memory, and effector subsets. The proportion of T helper cells ($CD4^+$) increased over time in both genotypes, with both reaching a peak at later ages (17 to 20 months and beyond), although both groups tended to show a reduced percentage in the adult stage (8 to 10 months). In contrast, the proportion of cytotoxic T cells ($CD8^+$) decreased over time in both genotypes (Fig. 1D). Naïve T helper cells ($CD4^+$ $CD44^-$ $CD62L^+$) peaked at 8 to 10 months old in both genotypes before decreasing, with minimal levels observed at >24 months. This trend was consistent between the two groups, with no significant differences observed. Memory T helper cells ($CD4^+$ $CD44^+$ $CD62L^-$) initially maintained stable levels in both mouse cohorts but declined by the later stages (17 to 20 and >24 months). Effector T helper cells ($CD4^+$ $CD44^+$ $CD62L^+$) fluctuated over time, with both groups displaying similar patterns. The proportion decreased at 8 to 10 months and increased thereafter, with minor differences between genotypes. Taking these three subsets together, we can observe that in both mouse cohorts, at the adult age, the percentage of naïve T helper cells increases notably, and as a compensation mechanism, effector T helper cells are substantially decreased (Fig. 1E). Cytotoxic naïve T cells ($CD8^+$ $CD44^-$ $CD62L^+$) also peaked at 8 to 10 months in both groups before declining in later stages. Cytotoxic memory T cells ($CD8^+$ $CD44^+$ $CD62L^-$) exhibited stable levels across all time points, with no significant differences between the genotypes. Cytotoxic effector T cells ($CD8^+$ $CD44^+$ $CD62L^+$) displayed an increasing trend with age, peaking at >24 months. However, the transgenic group reached a significantly higher proportion in the later stages compared with the wild type. Also, the proportion decreased at 8 to 10 months in both genotypes. Taking these three subsets together, we can also observe that in both mouse cohorts, at the adult age, the percentage of cytotoxic naïve T cells increases notably, compensated by a substantial decrease in cytotoxic effector T cells, as memory cells display a constant pattern. In summary, we have found that in both genotypes, $CD4^+$ T helper cells increased with age, peaking at later stages, while $CD8^+$ cytotoxic T cells decreased over time. Both T helper and cytotoxic T cell subsets showed a peak in naïve cells at the adult stage (8 to 10 months), balanced by a decrease in effector cells, with notable increases in effector cytotoxic T cells in the transgenic group at advanced ages (Fig. 1F).

We measured oxygen consumption (mitochondrial and nonmitochondrial) in Bcl-xL–overexpressing T cells and their controls. Mitochondrial proton leak was substantially diminished in Bcl-xL–overexpressing T cells (Fig. 2A). Basal respiration was also lower in Bcl-xL–overexpressing T cells than in the controls, indicating less oxygen requirement (probably because of the higher mitochondrial efficiency, as indicated by lower proton leak) (Fig. 2B). We also determined nonmitochondrial oxygen consumption (NMOC), which was diminished, especially in young Bcl-xL–overexpressing T cells (Fig. 2C). Much of NMOC is due to the action of oxygenases and oxidases, both of which generate reactive oxygen species. We thus measured lipid peroxidation in T cells and found that it fell from 9.88 to 5.07 μmol/mg of protein in the group of 8 to 10 months of age (Fig. 2D).

We measured caspase 9 as an indicator of intrinsic apoptosis, which was significantly decreased in old (17 to 20 months old) transgenic mice compared to wild-type mice (Fig. 2E). We then evaluated the capacity of T cells overexpressing Bcl-xL to survive in vitro under basal and stressful conditions, such as dexamethasone treatment or upon serum removal for 4, 24, and 48 hours (Fig. 2F). T cells overexpressing Bcl-xL were more resistant to stress-induced apoptosis at young and adult ages compared to wild-type T cells.

Last, we evaluated the cytokine production by T cells stimulated with phorbol 12-myristate 13-acetate (PMA)/ionomycin for 24 hours. Interleukin-1β (IL-1β) levels increased progressively with age in control T cells but remained constant in transgenic T cells. Therefore, control T cells produced significantly higher levels of IL-1β at older ages (17 to 20 and >24 months). IL-6 levels remained constant across aging, and no differences between wild-type and transgenic T cells were observed. Tumor necrosis factor–α (TNFα) levels showed an increasing tendency with age in control T cells. By contrast, TNFα levels decreased progressively with age in transgenic T cells. At very old ages (>24 months), control T cells produced significantly higher levels of TNFα compared to transgenic T cells. Interferon-γ (IFN-γ) levels displayed an increasing pattern with aging in both wild-type and transgenic T cells. However, control T cells produced significantly higher levels of IFN-γ than transgenic T cells at all ages. Together, T cells overexpressing Bcl-xL produce significantly lower levels of pro-inflammatory cytokines than control T cells, especially at older ages (Fig. 2G).

Overall, Bcl-xL overexpression does not modify T cell subsets but promotes a more efficient metabolism, an improved resistance to stress-induced apoptosis, and a less pro-inflammatory secretion pattern.

Bcl-xL overexpression boosts macroautophagy in T cells upon nutrient deprivation

We then decided to focus on nutrient deprivation because it is a natural enhancer of autophagy. When we used NH_4Cl/leupeptin (N/L) to inhibit proteolysis in lysosomes and analyzed the increase in Bcl-xL at different times, we noted that Bcl-xL undergoes degradation in lysosomes under basal conditions and that this lysosomal degradation is further enhanced upon serum removal (Fig. 3A). Conversely, Bcl-xL affects lysosomal activity. We used NIH3T3 cells overexpressing Bcl-xL and transfected them with the mCherry-GFP-LC3 macroautophagy reporter that allows monitoring changes in the number of autophagosomes (positive for both fluorophores) and maturation of autophagosomes into autolysosomes upon fusion with lysosomes [positive for mCherry only, because green fluorescent protein (GFP) is quenched by the acidic pH]. We found increased autophagic flux in cells expressing Bcl-xL, as demonstrated by a significantly higher number of autolysosomes with a

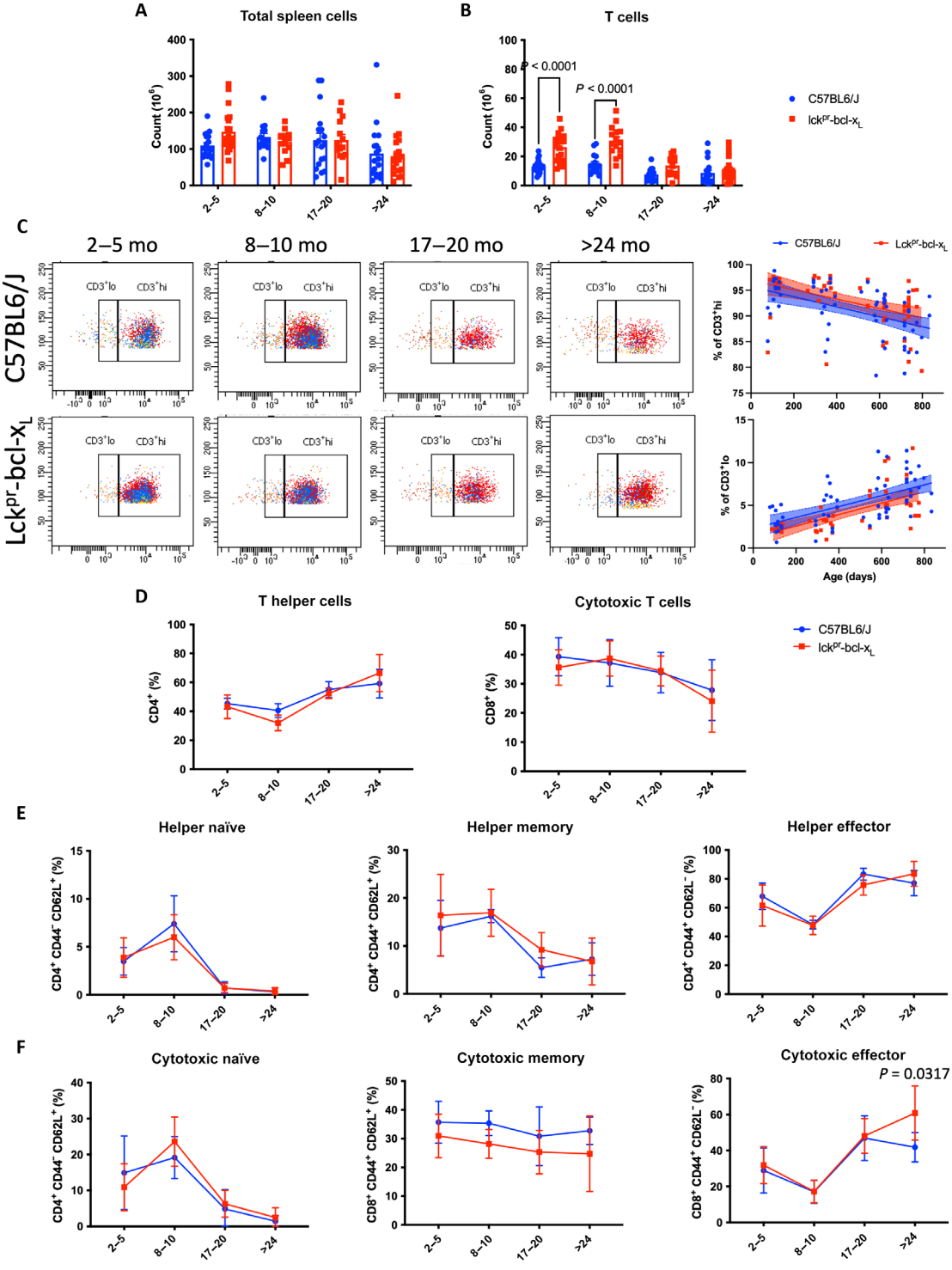

Fig. 1. Bcl-xL overexpression alters T cell populations in Lck^{pr}-bcl-x$_L$ mice across aging. (**A**) Total splenic cell counts and (**B**) T cell count obtained from the spleens of C57BL6/J and Lck^{pr}-bcl-x$_L$ mice of all age groups (n = 15 to 20). (**C**) CD3$^+$hi and CD3$^+$lo levels of splenic T cells from C57BL6/J and Lck^{pr}-bcl-x$_L$ mice of all age groups (n = 15). mo, months. (**D**) Distribution of T helper and cytotoxic T cells, (**E**) distribution of naïve/memory/effector within T helper cells, and (**F**) distribution of naïve/memory/effector within cytotoxic T cells in C57BL6/J and Lck^{pr}-bcl-x$_L$ mice of all age groups (n = 8 to 10). Data are presented as the means ± SD.

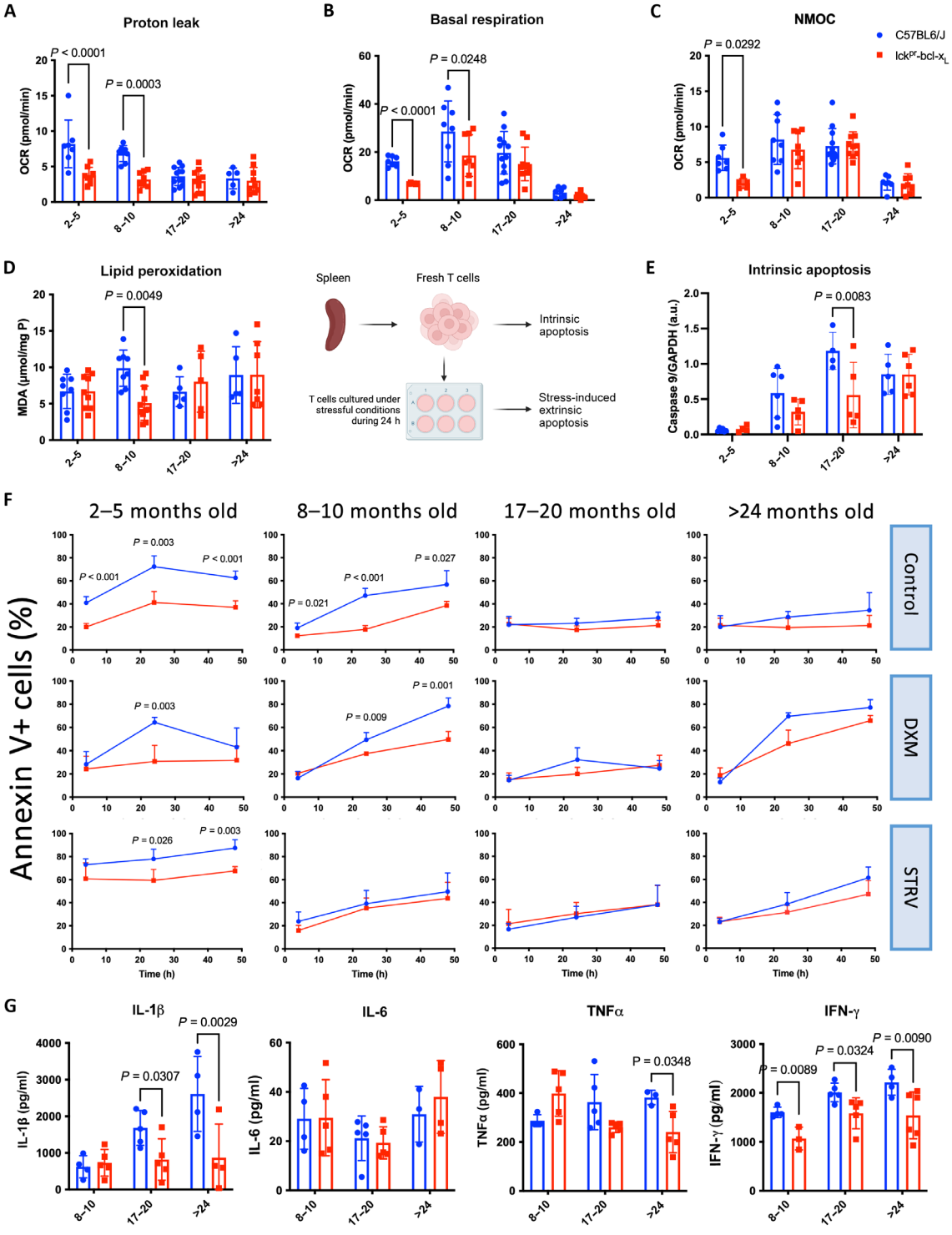

Fig. 2. Bcl-xL improves metabolic performance, induces apoptosis resistance of T cells, and modulates cytokine production. (**A**) Proton leak, (**B**) basal respiration, and (**C**) NMOC of splenic T cells from C57BL6/J and Lck^{pr}-bcl-x$_L$ mice of all age groups (n = 8 to 12). (**D**) Lipid peroxidation of splenic T cells from C57BL6/J and Lck^{pr}-bcl-x$_L$ mice of all age groups (n = 5 to 9). h, hours. (**E**) Intrinsic apoptosis (caspase 9) of isolated T cells and (**F**) stress-induced extrinsic apoptosis (annexin V) of T cells cultured in vitro during 48 hours under control and dexamethasone (100 nM) or upon serum removal (n = 5 to 6). a.u., arbitrary units. (**G**) Cytokine production (IL-1β, IL-6, TNFα, and IFN-γ) by cultured T cells upon 24 hours of stimulation with PMA/ionomycin (n = 4 to 5). Data are presented as the means ± SD.

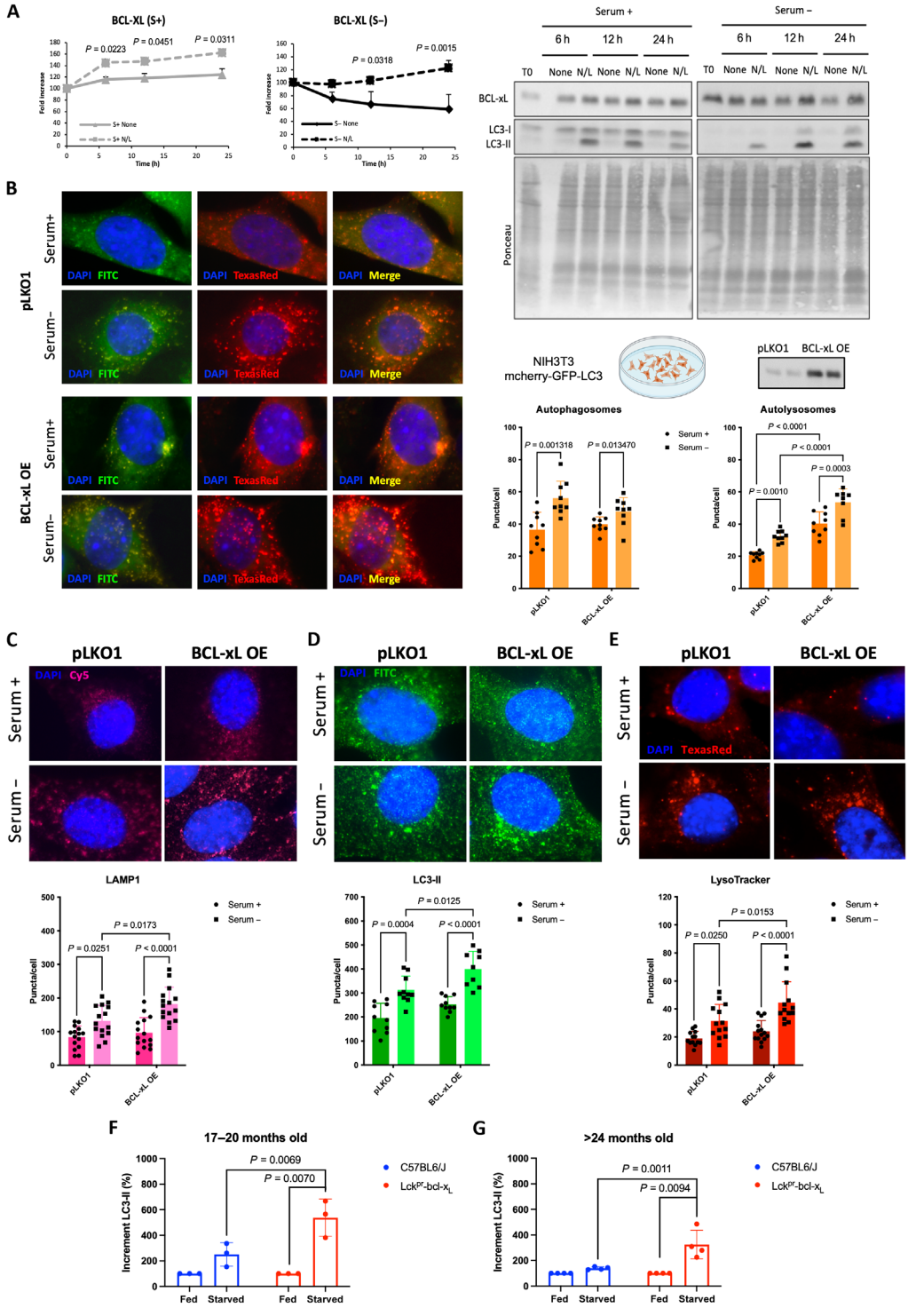

Fig. 3. Bcl-xL boosts macroautophagy under starvation conditions. (**A**) Bcl-xL lysosomal degradation in MEFs maintained in the presence or absence of serum during 24 hours ($n = 6$ independent experiments). (**B**) Bcl-xL effect on macroautophagy measured in NIH3T3 mouse fibroblasts stably expressing Bcl-xL or the pLKO1 control vector and transfected with the macroautophagy reporter (mCherry-GFP-LC3). Cells were maintained in serum-supplemented (+) or serum-deprived (–) culture media. Yellow puncta ($mCherry^+/GFP^+$) represent autophagosomes, and red puncta ($mCherry^+/GFP^-$) represent autolysosomes ($n = 9$ fields with $n > 15$ cells). (**C** to **E**) Immunofluorescence for LAMP1 (C), LC3-II (D), and LysoTracker staining (E) in NIH3T3 cells stably expressing Bcl-xL or the pLKO1 vector control and cultured in the presence (+) or absence (–) of serum ($n = 10$ to 15 fields with $n > 10$ cells). (**F** and **G**) LC3-II levels of splenic T cells from (F) old and (G) very old C57BL6/J and Lck^{pr}-bcl-x_L mice cultured in the presence or absence of serum ($n = 3$ to 4). Data are presented as the means ± SD.

comparable number of autophagosomes, in support of efficient autophagy (Fig. 3B). Accordingly, while under basal conditions (serum+), we did not find significant differences between control and Bcl-xL–expressing cells in levels of lysosomal-associated membrane protein 1 (LAMP1), autophagy-related protein light chain 3 (LC3)-II, and LysoTracker; levels of these three markers of the autophagic/lysosomal compartment were significantly higher in Bcl-xL–transfected cells upon nutrient removal (Fig. 3, C to E). Thus, Bcl-xL overexpression boosts basal and inducible macroautophagy flux and associates with an adaptative expansion of autophagic/lysosomal compartments under starvation conditions.

We then verified these findings in vivo using splenic T cells isolated from our mouse cohorts at different ages. Analysis of LC3-II flux demonstrates the described inability of T cells from old wild-type mice to up-regulate macroautophagy in response to nutritional stress (starvation), while T cells from mice overexpressing Bcl-xL showed preserved response to starvation (Fig. 3, F and G).

Overall, our findings support a tight interplay between Bcl-xL and autophagy, where the stimulatory effect of this protein over serum deprivation–induced autophagy may be self-regulated through its own lysosomal degradation.

Bcl-xL overexpression may support muscle regeneration by promoting T cell infiltration in skeletal muscle and potentially reducing IFN-γ–mediated inflammation

A proper interaction between skeletal muscle cells and immune cells enables the regenerative potential of skeletal muscle. In response to injury, immune cells infiltrate skeletal muscle to restore muscle homeostasis by removing damaged cells and by secreting growth factors needed for satellite cell proliferation and differentiation (*15*). The physiological functions of immune cells are gradually lost during aging, leading to the alteration of the cross-talk between the immune system and muscle cells, which likely contributes to decreased muscle regeneration with age. For an appropriate differentiation of muscle stem cells into myofibers, a shift from a pro-inflammatory to anti-inflammatory phenotype of immune cells is required. A major subset of T cells infiltrating skeletal muscle is FoxP3$^+$ T regulatory (T_{reg}) cells, which control muscle inflammation after tissue damage by releasing anti-inflammatory molecules.

T_{reg} cell homeostasis is impaired in old mice because of increased turnover rates and reduced recruitment from the circulating T cell pool (*16*). We thus analyzed T_{reg} cell distribution in our mouse cohorts. We observed that T_{reg} cell distribution in wild-type mice tends to accumulate in the spleen with age; however, in transgenic mice, T_{reg} cells do not accumulate in the spleen and are released to the circulating pool in the blood (Fig. 4, A and B). We then observed an increased infiltration of CD3$^+$ T cells in the skeletal muscle of wild-type animals with aging compared to transgenic animals, where levels of CD3$^+$ T cells remained constantly low. However, in proportion, the number of T_{reg}-infiltrated cells was significantly higher in transgenic mice at older ages (Fig. 4, C to F).

It has been reported that T_{reg} cells modulate IFN-γ production (*17*). This observation is of particular interest in the context of muscle aging because IFN-γ is known to increase with aging and to be actively contributing to age-related tissue damage (*18*). We confirmed it in our mouse cohorts (Fig. 4G). IFN-γ levels were increased in wild-type mice with age; however, mice overexpressing Bcl-xL displayed constant levels of IFN-γ upon aging. At very old ages (>24 months), transgenic mice showed significantly lower levels of IFN-γ than controls.

Local injection of $BaCl_2$ is an established model of acute injury to study skeletal muscle regeneration. To examine the temporal changes in histological morphologies of gastrocnemius muscle after $BaCl_2$-induced muscle injury, we harvested gastrocnemius muscle at 4 and 10 days after $BaCl_2$ local injection (Fig. 5A). Upon $BaCl_2$ injection, muscle fibers rapidly degenerated; therefore, at 4 days postinjection, the muscle fiber diameter decreased significantly in both control and transgenic mice. Also, at this stage, newly formed myotubes with central nuclei have smaller diameters compared to mature muscle fibers. Transgenic mice display a significantly higher percentage of central nuclei. As regeneration progresses, myotubes mature and gradually increase in diameter. At 10 days postinjection, the muscle fiber diameter of transgenic mice has already recovered the original size of uninjured fibers, while control mice still display smaller diameters (Fig. 5, B and C).

Overall, transgenic mice showed reduced IFN-γ levels and a more effective T_{reg} recruitment compared to wild-type mice, maintaining muscle regenerative potential during aging. Following injury, transgenic mice exhibited faster recovery of muscle fiber size, suggesting a protective role in aging-related muscle repair. Together, Bcl-xL overexpression in T cells enhances muscle regeneration, possibly due to increased T_{reg} cell infiltration and lower age-related IFN-γ inflammation in skeletal muscle.

Bcl-xL overexpression in T cells prevents age-associated muscle mitochondrial structural and functional decay

Aging is characterized by a progressive loss of muscle mass and energy (*19*). Hence, we first assessed the quality of muscle mitochondria across the aging of our mice overexpressing Bcl-xL exclusively in T cells (Lck^{pr}-bcl-x_L). To this aim, we observed the mitochondrial outer membrane integrity and crista density of intermyofibrillar mitochondria of gastrocnemius muscles. Figure 6A depicts that the mitochondrial structure from wild-type animals changed with aging, showing morphological abnormalities such as a discontinuous outer membrane or defective cristae when compared to transgenic mice, which maintain the younger phenotype. The quantification of these images revealed that transgenic mice maintained mitochondrial membrane integrity through aging, whereas control mice displayed a significantly higher ratio of membrane discontinuity already at adult ages. Similarly, wild-type mice consistently show a lower crista density, whereas transgenic mice maintain a higher number of cristae per unit area with age (Fig. 6B). However, there were no differences in mitochondrial biogenesis or mitochondrial quantity (Fig. 6C) between wild-type and transgenic mice during aging.

Respiratory chain complexes are packed into functional supercomplexes within the folds of the inner mitochondrial membrane. Respiratory function and mitochondrial ultrastructure are closely related as crista shape determines the assembly and stability of the supercomplexes and, hence, mitochondrial respiratory efficiency (*20*). To better understand the nature of the predicted mitochondrial impairment, we assessed mitochondrial respiratory capacity using a multiple substrate-uncoupler-inhibition titration (SUIT) protocol to measure high-resolution respirometry. In general, the oxygen consumption rate (OCR) diminished with aging in different coupling states. As observed in Fig. 6D, adult mice (8 to 10 months old) showed maximum OCR values around 80 pmol/(s ml), whereas old mice (17 to 20 months old) only reached 60 pmol/(s ml). The addition of succinate to test oxidative phosphorylation (OXPHOS) capacity and maximum coupled respiration from both complexes I and

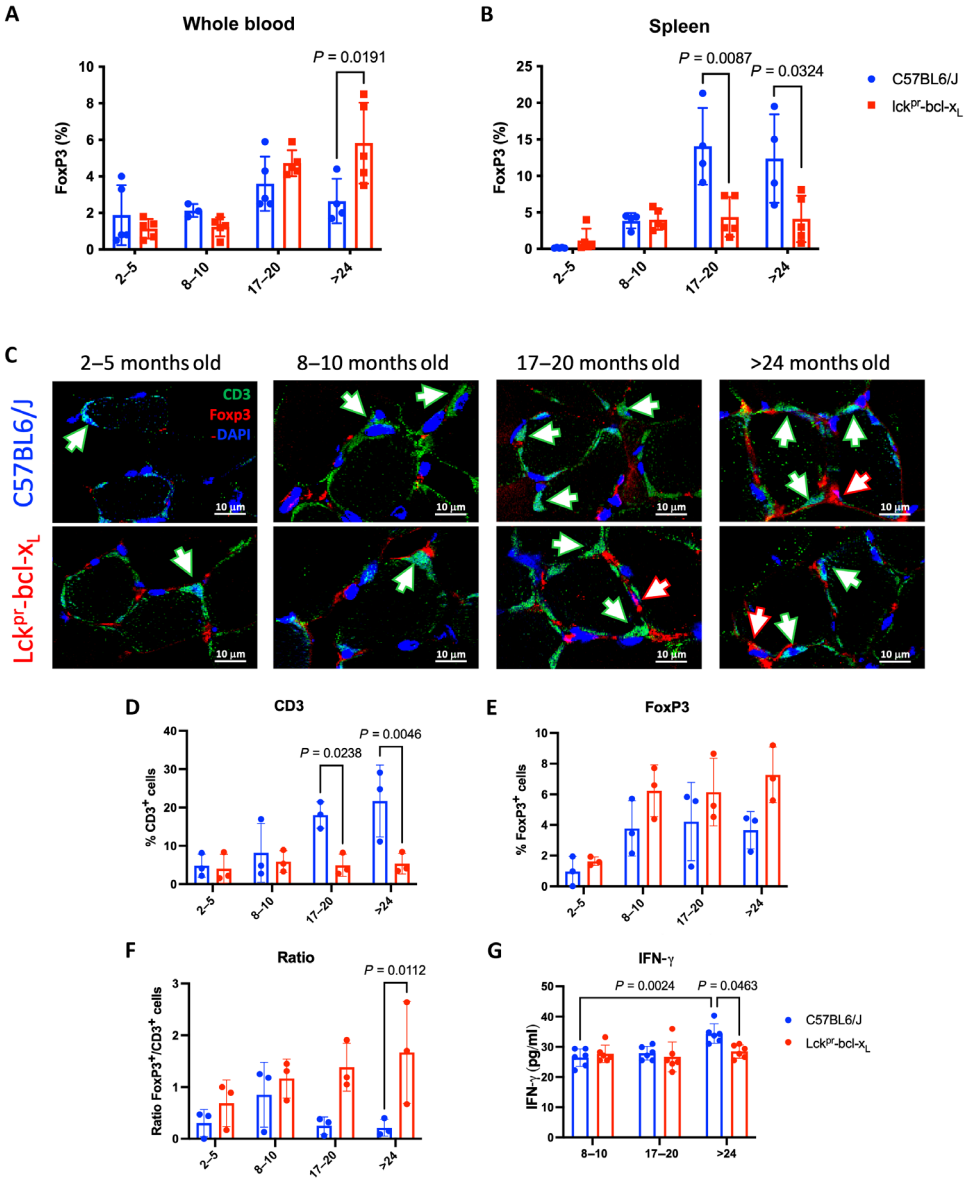

Fig. 4. Bcl-xL overexpression modulates T_{reg} distribution and promotes T_{reg} infiltration in skeletal muscle to reduce IFN-γ inflammation. Percentage of FoxP3$^+$ T_{reg} cells in (**A**) whole blood and in (**B**) spleens from C57BL6/J and Lck^{pr}-bcl-x_L mice of all age groups ($n = 4$ to 5). (**C**) Representative images of CD3$^+$, FoxP3$^+$, and DAPI staining in muscle samples from C57BL6/J and Lck^{pr}-bcl-x_L mice of all age groups. Quantification of (**D**) infiltrated CD3$^+$ cells and (**E**) FoxP3$^+$ cells and (**F**) ratio of FoxP3$^+$/CD3$^+$ ($n = 3$ fields with $n > 50$ cells). (**G**) IFN-γ levels measured in plasma from C57BL6/J and Lck^{pr}-bcl-x_L mice ($n = 6$). Data are presented as the means ± SD.

II (OXPHOS CI and CII) revealed that both were significantly higher in transgenic mouse mitochondria. Next, after the addition of an exogenous uncoupler, carbonyl cyanide ptrifluoromethoxyphenylhydrazone (FCCP), to collapse the proton gradient, the maximum electron transfer capacity [electron transport system (ETS) CI and CII] was found to be again significantly increased in transgenic mouse mitochondria. Last, the addition of rotenone, a complex I inhibitor, revealed that the submaximal ETS CII respiratory state was also improved in transgenic mouse mitochondria. All these differences between wild-type and transgenic mice were significant in mitochondria from adult mice, while in the old mouse group, only OXPHOS CI and CII were significantly higher in the transgenic mice.

To test whether these better-functioning mitochondria produce a lesser amount of oxidative stress and damage, we measured lipid peroxidation (Fig. 6E) and protein carbonylation (Fig. 6F) in whole gastrocnemius samples. Transgenic mice showed reduced levels of lipid and protein oxidation at old ages (17 to 20 months), but only protein carbonylation levels remained significantly lower until very old age (>24 months).

Overall, Bcl-xL overexpression in T cells preserves the muscle mitochondrial structure and function during aging, preventing age-related membrane and crista degradation. Muscle mitochondria isolated from transgenic mice maintained higher respiratory efficiency, with increased OXPHOS and ETS capacities compared

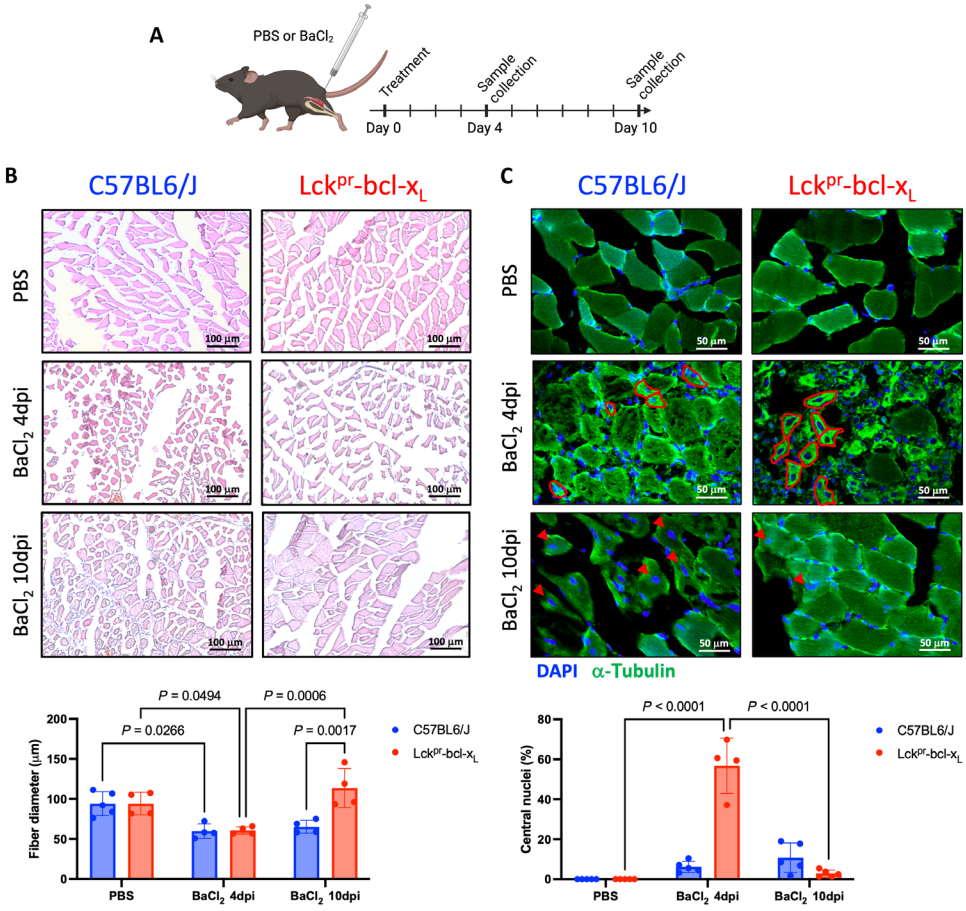

Fig. 5. Mice overexpressing Bcl-xL in T cells display improved muscle regeneration following $BaCl_2$ injury. (**A**) Diagram of the study design. (**B**) Representative images of hematoxylin and eosin staining and quantification of the mean muscle fiber diameter from C57BL6/J and Lck^{pr}-bcl-x_L mice treated with PBS or $BaCl_2$ ($n = 5$ fields with $n > 100$ fibers). (**C**) Representative images of DAPI and α-tubulin staining and quantification of central nuclei in muscle fibers from C57BL6/J and Lck^{pr}-bcl-x_L mice treated with PBS or $BaCl_2$ ($n = 5$ fields with $n > 100$ fibers). Nascent myotubes with central nuclei are highlighted in red. Mature myotubes with central nuclei are indicated with red arrows. Data are presented as the means ± SD. Abbreviation: dpi, days postinjection.

to wild-type mice, leading to lower oxidative damage, thus suggesting a protective effect against age-induced mitochondrial dysfunction.

Bcl-xL overexpression in T cells improves health span and reduces frailty in mice

Physical performance declines with increasing age and is used as a predictor of clinical outcome, mortality, and longevity in humans and rodents. We measured mice's body weight, forelimb grip strength, latency time to fall from a rotating rod (as an indicator of motor coordination), and running time during an incremental treadmill test (as a parameter of exercise endurance) in our cohort of young mice (*21*).

The forelimb grip strength test may be used to assess skeletal muscle function. We calculated the grip strength loss at different ages. As the animals grew older, we observed an increased percentage of grip strength loss in both genotypes (Fig. 7A). However, this grip strength loss was milder in transgenic adult mice (8 to 10 months). Motor coordination also follows a general decline in mice with aging. We calculated the percentage of latency time loss at different ages. Compared to control mice, transgenic mice showed a reduced loss of latency time in both the adult and old age groups, which maintain values comparable to those observed in the young group (Fig. 7B). Similar to the previous physical parameters, exercise endurance, measured as running time, also declines with advancing age. We found that the running times remained similar to values recorded at a young age until >24 months when the loss of physical endurance was more noticeable but to a similar extent in both genotypes (Fig. 7C).

The main aim of our research was to assess whether Bcl-xL overexpression in T cells may reduce or prevent frailty. To accomplish this, cutoff values of the aforementioned physical tests (forelimb grip strength, latency time to fall from a rotating rod, and running time during incremental treadmill test) performed at 17 to 20 and >24 months of age were used to calculate the prevalence of frailty and the Valencia frailty score for experimental animals developed by our group (*21*, *22*) and later validated by others (*23*). Valencia frailty score was significantly lower (better performance) in transgenic mice (11.11%) compared to wild-type mice (29.41%) at >24 months of age (Fig. 7D). Hence, Bcl-xL–overexpressing mice are less frail than their wild-type littermates.

To further evaluate the prevalence of frailty, we categorized each mouse as nonfrail, prefrail, or frail according to the number of met criteria at >24 months of age (*21*). Of the 18 transgenic

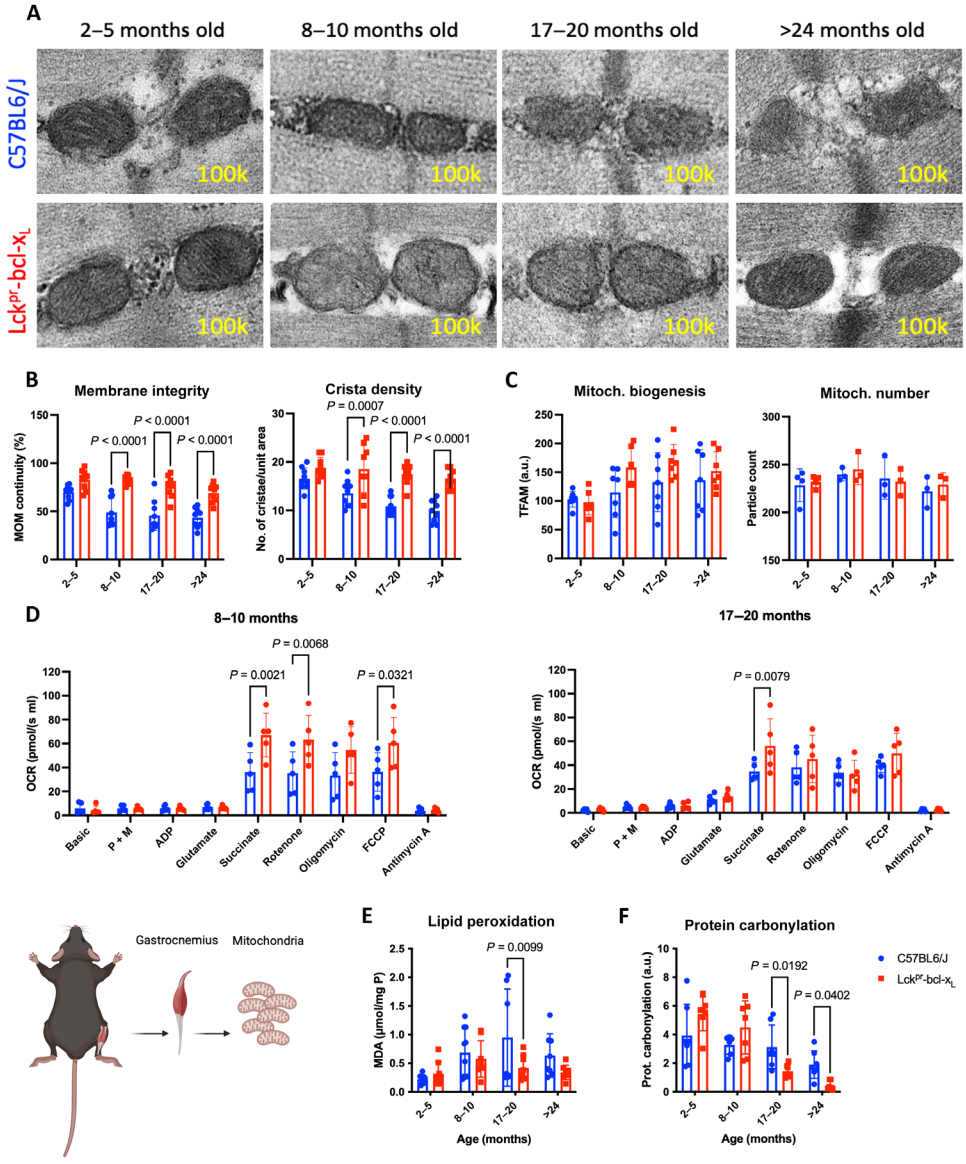

Fig. 6. Mice overexpressing Bcl-xL in T cells maintain the muscle mitochondrial structure and function and prevent oxidative damage during aging. (**A**) Representative electron microscopy images of muscle mitochondria from C57BL6/J and Lck^{pr}-bcl-x$_L$ mice at the indicated age ranges. (**B**) Quantification of the mitochondrial structure as of mitochondrial outer membrane integrity and crista density ($n = 7$ fields with $n > 20$ mitochondria). (**C**) TFAM protein levels ($n = 7$) and mitochondrial count in muscle samples of C57BL6/J and Lck^{pr}-bcl-x$_L$ mice of all age groups ($n = 3$ to 4 fields with $n > 200$ mitochondria). (**D**) Muscle mitochondrial bioenergetics of adult and old C57BL6/J and Lck^{pr}-bcl-x$_L$ mice ($n = 5$). (**E**) MDA levels and (**F**) protein carbonylation levels of muscle samples of C57BL6/J and Lck^{pr}-bcl-x$_L$ mice of all age groups ($n = 7$). Data are presented as the means ± SD.

mice, only 1 was prefrail, and none was frail. In contrast, of the 17 wild-type mice, 6 were prefrail, and 2 were frail. The number of nonfrail transgenic mice almost doubled the number of nonfrail wild-type mice (Fig. 7E). This frequency distribution was statistically significant.

We then performed a microscopic analysis to assess the muscle quality of our mouse cohorts (Fig. 7F). We detected an increased cross-sectional area of muscle fibers (Fig. 7G) as well as a higher protein content (Fig. 7H) in samples from old mice (17 to 20 months of age) overexpressing Bcl-xL in T cells. Together, Bcl-xL overexpression in T cells preserves muscle health and prevents frailty in mice at advanced ages.

Bcl-xL overexpression in T cells maintains metabolic performance during aging

C57BL/6J mice's body weight is known to increase with increasing age (*21*). We measured the body weight at different ages and computed the percentage of body weight gain from 2 to 5 months of age. Although we observed a general increase in body weight gain above 25% in both strains at all age groups compared to the initial values at 8 to 10 and 17 to 20 months of age, transgenic Lck^{pr}-bcl-x$_L$ mice showed significantly lower body weight gain compared to wild-type mice (Fig. 8A).

Changes in body composition during aging are due in part to changes in the balance between physical activity and energy intake

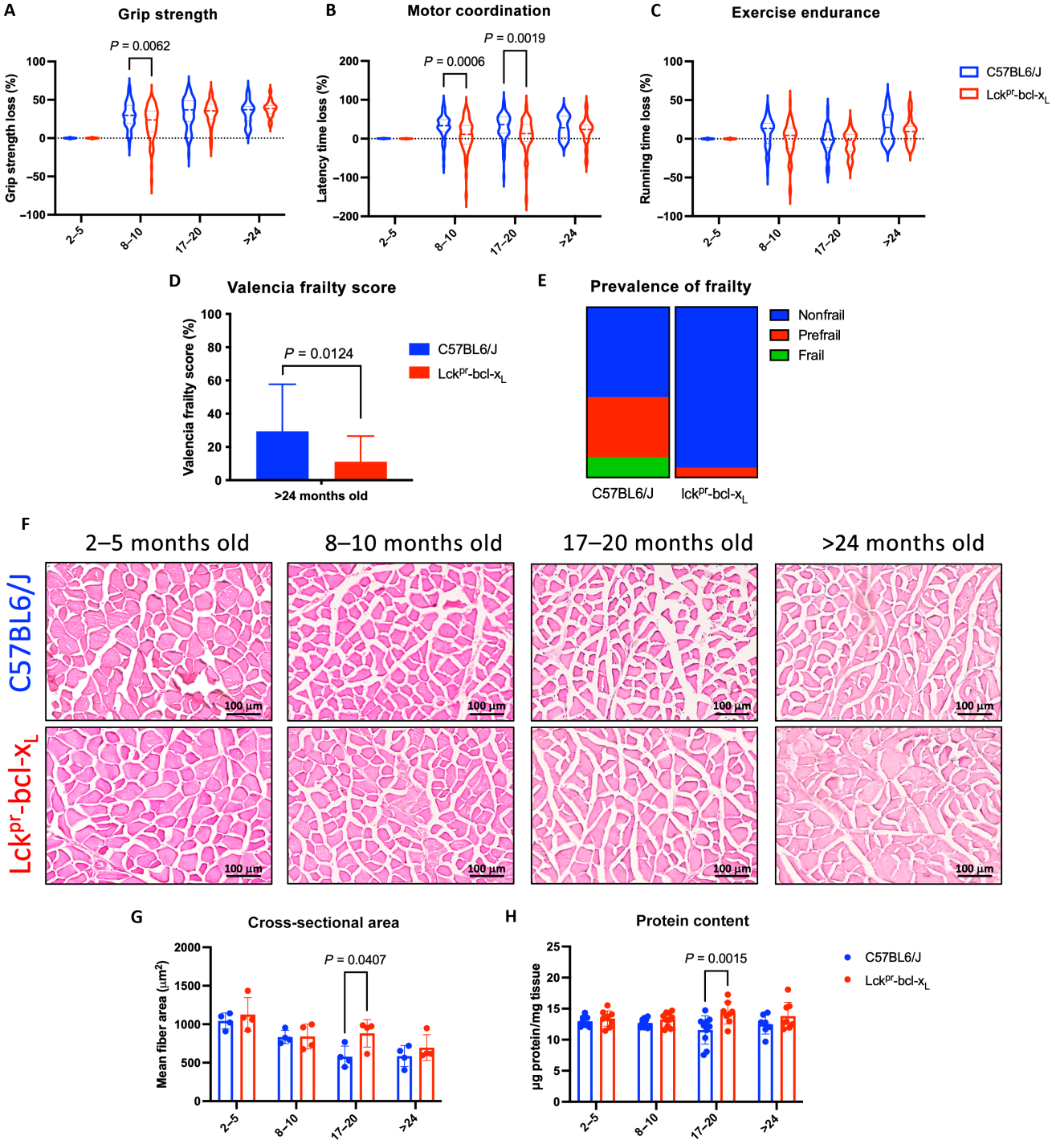

Fig. 7. Mice overexpressing Bcl-xL in T cells display increased grip strength and motor coordination, making them less frail. (**A**) Grip strength loss, (**B**) motor coordination loss, and (**C**) exercise endurance loss of 8 to 10 ($n = 135$)–, 17 to 20 ($n = 116$)–, and >24 ($n = 34$)–month-old C57BL6/J and Lck^{pr}-bcl-x$_L$ mice. Reference values are C57BL6/J and Lck^{pr}-bcl-x$_L$ mice of 2 to 5 months old ($n = 135$). There were no differences in the absolute values of grip strength, motor coordination, or exercise endurance across the two young animal groups. (**D**) Prevalence of frailty in >24-month-old C57BL6/J and Lck^{pr}-bcl-x$_L$ mice. C57BL6/J nonfrail ($n = 9$), prefrail ($n = 6$), and frail ($n = 2$); Lck^{pr}-bcl-x$_L$ nonfrail ($n = 17$), prefrail ($n = 1$), and frail ($n = 0$). Data are presented as mosaic plots, and $P = 0.01244$ was calculated with Fisher's exact test. (**E**) Valencia frailty score in >24-month-old C57BL6/J ($n = 17$) and Lck^{pr}-bcl-x$_L$ ($n = 18$) mice. (**F**) Representative images of hematoxylin and eosin staining of muscle fibers from C57BL6/J and Lck^{pr}-bcl-x$_L$ mice of all age groups. (**G**) Quantification of the mean cross-sectional area of muscle fibers ($n = 4$ fields with $n > 100$ fibers) and (**H**) total protein content ($n = 7$) in the muscle of C57BL6/J and Lck^{pr}-bcl-x$_L$ mice of all age groups. Data are presented as the means ± SD.

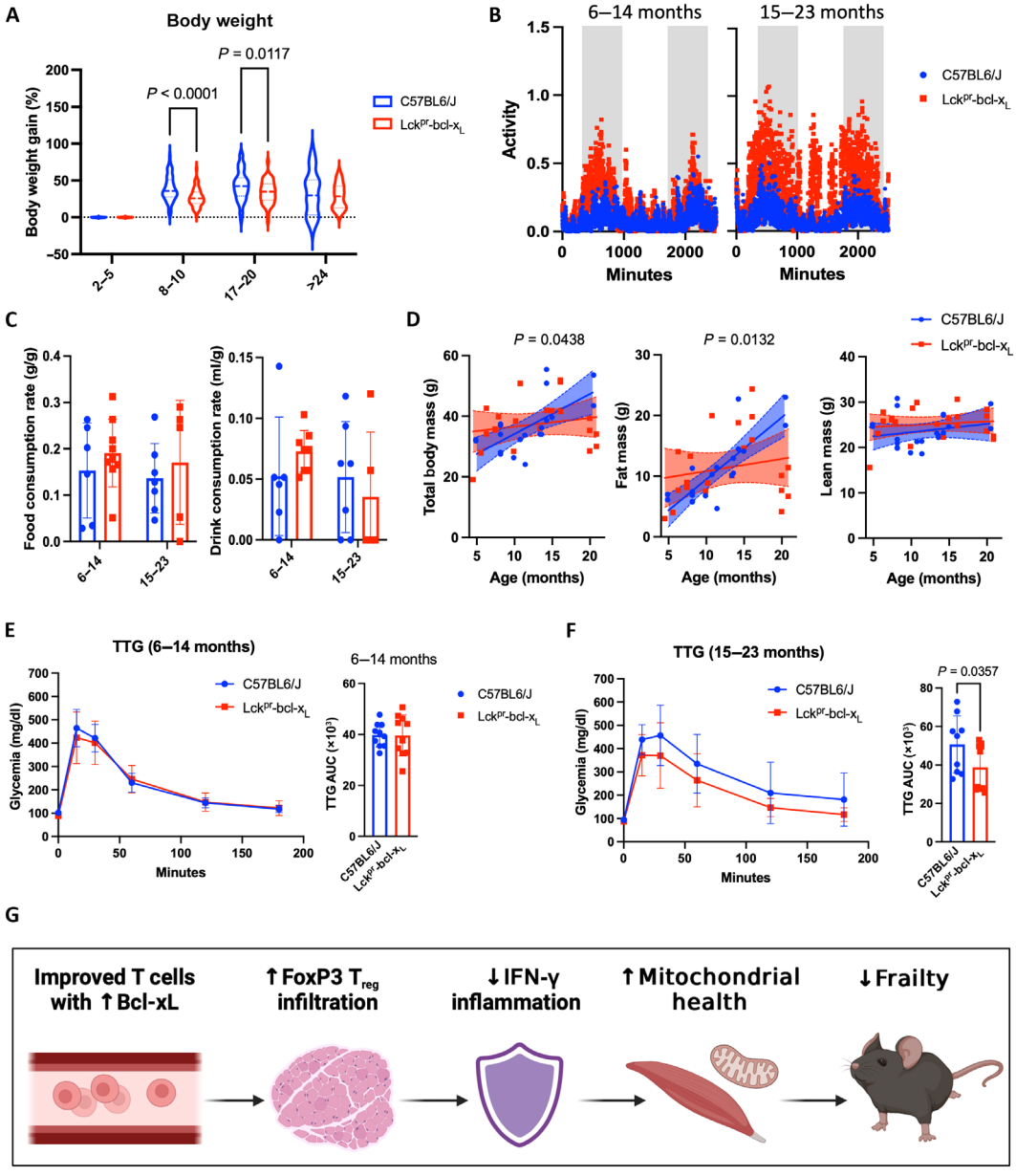

Fig. 8. Mice overexpressing Bcl-xL in T cells are more metabolically competent at old ages. (**A**) Body weight gain of 8 to 10 ($n = 135$)–, 17 to 20 ($n = 116$)–, and >24 ($n = 34$)–month-old C57BL6/J and Lck^{pr}-bcl-x$_L$ mice. Reference values are C57BL6/J and Lck^{pr}-bcl-x$_L$ mice of 2 to 5 months old ($n = 135$). (**B**) Spontaneous activity measured as horizontal activity in C57BL6/J ($n = 6$) and Lck^{pr}-bcl-x$_L$ ($n = 9$) mice over 42 hours at the indicated ages. (**C**) Food and drink consumption in C57BL6/J and Lck^{pr}-bcl-x$_L$ mice at the indicated ages ($n = 5$ to 7). (**D**) Regression curves for total body mass, fat mass, and lean mass of C57BL6/J and Lck^{pr}-bcl-x$_L$ mice during aging ($n = 15$ to 20 per group). Glucose tolerance test: glycemia evolution and glycemia area under the curve (AUC) analysis in C57BL6/J and Lck^{pr}-bcl-x$_L$ mice of (**E**) 6 to 14 months ($n = 10$) and (**F**) 15 to 23 months ($n = 9$). Data are presented as the means ± SD. (**G**) Rendition of the findings reported.

(*21*). We observed that wild-type mice displayed less spontaneous physical activity than controls, especially at older ages (Fig. 8B). Next, we determined our mice's daily energy intake (Fig. 8C) and body composition (Fig. 8D) across ages. Despite no differences in food and drink consumption between wild-type and transgenic mice, we observed a general gain in total body mass that was exacerbated in wild-type mice. This increase was mainly due to an accumulation of fat mass in these animals with aging (Fig. 8D). We conclude then that the reduced weight gain in the transgenic mice was not a consequence of reduced food consumption but rather of higher energy expenditure because of their sustained higher physical activity with age (*21*).

Last, we also evaluated the metabolic function by performing a glucose tolerance test (*21*). No differences were observed between wild-type and transgenic mice in younger animals (Fig. 8E). However, older wild-type mice showed the highest values of glycaemia during the recovery phase (Fig. 8F). The area under the curve (AUC) analysis confirmed an improved glucose tolerance in aged (15 to 23 months old) transgenic mice compared to the corresponding controls.

Together, T_{reg} cells overexpressing Bcl-xL could act as shields preventing the accumulation of IFN-γ–mediated damage with aging, thereby promoting muscle mitochondrial health, which may be in part through the enhancement of autophagy, and reducing frailty (Fig. 8G).

DISCUSSION

Bcl-xL: From centenarians to mice and cells

This study stemmed from our prior work indicating that Bcl-xL emerges as a significant gene exhibiting differential expression between centenarians, octogenarians, and younger individuals (*4*). Given Bcl-xL's involvement in mitochondrial metabolism and function (*24*) and the important role of the immune system in aging, we undertook an analysis of the consequences of its overexpression exclusively in T cells. T cells were chosen because of their representation of polymorphonuclear cells, the only nucleated cell type feasible for transcriptomic analysis in centenarian individuals because of practical and ethical constraints. Hence, this is an example of reverse translational research in which information obtained in humans is validated in animals in vivo and also in cultured cells in vitro.

Our primary aim here was to show the possible mechanistic relationship between Bcl-xL expression and our previously reported major role of Bcl-xL in successful aging and resilience promotion across the animal kingdom, from *Caenorhabditis elegans* to mice and humans (*4*).

Bcl-xL improves T cells' resilience during aging

T cell aging plays a major role in body-wide deterioration. Among the described hallmarks of T cell aging (*25*), we detected some of them, including thymic involution and mitochondrial dysfunction. Mitochondria from wild-type T cells exhibited impaired OXPHOS in the absence of changes in biogenesis or mitochondrial number, thus suggesting that dysfunctional mitochondria accumulate because of the inefficient turnover through mitophagy. Moreover, mitochondrial dysfunction in T cells can contribute to a secretory phenotype (releasing molecules such as mitochondrial DNA, ATP, cardiolipin, and *N*-formyl-peptides), leading to the establishment of a pro-inflammatory milieu (*26*).

T cells obtained from mice overexpressing Bcl-xL, which is an antiapoptotic protein, exhibited decreased levels of apoptosis at young and adult ages, but no differences were found in the aged groups. This can be explained by the experiments performed by Boise *et al.*, which demonstrated that Bcl-xL levels were constant in resting T cells but were strongly induced in activated T cells (*27*–*29*). When cultured and submitted to different stresses, T cells from Bcl-xL–overexpressing mice were protected from apoptosis.

Deregulation of autophagy and apoptosis is a common hallmark of the aging process (*30*). In T cells, autophagy has an essential role in modulating protein and organelle homeostasis and the regulation of activation-induced responses, and autophagy has been shown preserved in T cells from centenarian families (*31*). Several studies have reported that members of families with exceptional longevity show improved immune function, which might contribute to the increased lifespan and health span observed in those families (*32*–*35*). Maintaining a proper autophagic function is necessary to adapt to stressful conditions. We found that Bcl-xL overexpression, both in NIH3T3 cells and also in T cells from Bcl-xL–overexpressing mice, is sufficient to boost the induction of macroautophagy in response to nutrient deprivation. These findings suggest that T cells overexpressing Bcl-xL are more capable of adapting to harsh conditions by modulating apoptosis and macroautophagy and that, probably, this boosting effect on autophagy may also contribute to timely mitochondrial turnover and overall better mitochondrial function. Thus, Bcl-xL overexpression supports a more resilient immune system.

Bcl-xL lowers IFN-γ inflammation and promotes muscle regeneration

It has been suggested that the accumulation of abdominal fat (visceral rather than subcutaneous) can establish and sustain a chronic low-grade inflammation (*36*). Bcl-xL animals, being leaner than their wild-type homologs, might be protected against the accumulation of pro-inflammatory cytokines released by an excessive amount of adipose tissue.

Beyond fat tissue, immune cells also contribute to the establishment of the systemic chronic, low-grade inflammation associated with aging. T cells obtained from our old wild-type animals produced higher levels of pro-inflammatory cytokines and displayed higher rates of dysfunctional mitochondria and impaired autophagy (*26*, *37*). Furthermore, senescent T cells have a preferential homing capacity for peripheral tissues, contributing to the establishment of a local chronic, low-grade inflammation (*38*), which correlates with our results showing a significant accumulation of T cells in muscle from wild-type animals with aging. We report that Bcl-xL–overexpressing mice maintain $CD3^+$ immune cell infiltration at levels found in the young animal, whereas old controls display an increase in these cells. Moreover, the proportion of $FoxP3^+$ cells (an anti-inflammatory subset of T cells) is increased in Bcl-xL mice. This shift to a more anti-inflammatory infiltration in Bcl-xL mice was more evident when we determined the $FoxP3^+/CD3^+$ ratio.

T_{reg} cells, particularly those of the $FoxP3^+$ subset, are critical modulators of the immune response. FoxP3 activates genes such as CD25 and CTLA-4, and at the same time, it inhibits the function of NFAT (nuclear factor of activated T cells) and nuclear factor κB (nuclear factor κB), which leads to the suppression of genes, including IL-2 and other effector T cell cytokines (*39*). T_{reg} cells are also important players in muscle regeneration as they accumulate in both acute and chronically injured muscle, where they promote satellite cell proliferation and the M1-to-M2 switch in macrophages, thereby changing from a pro- to anti-inflammatory ambient (*40*). T_{reg} cells represent about 10% of the $CD3^+$ T cell compartment in uninjured skeletal muscle of C57BL/6J mice, a frequency that decreases with age as a result of impaired recruitment and retention (*16*, *41*). However, the frequency of T_{reg} cells overexpressing Bcl-xL in muscle tissue increases with age, suggesting that these mice are protected against the establishment of local inflammation. It has been shown that the deletion of T_{reg} cells increases the presence of both $CD8^+$ and $CD4^+$ T cells in the heart injury zone, which is accompanied by an increased secretion of IFN-γ and TNFα, suggesting that T_{reg} cells not only decrease the infiltration of conventional T cells but also attenuate their activity (*42*).

It is also known that T_{reg} cells regulate the activity of skeletal muscle precursor cells and are instrumental in the proper regeneration of the tissue (*43*–*45*). Current studies have indicated that T_{reg} cells regulate muscle stem cells mostly through amphiregulin, a member of the epidermal growth factor family that stimulates the proliferation of most cell types (*16*, *46*).

Recently, a study uncovered the T_{reg}-IFN-γ-mitochondria pathway involvement in muscle inflammation during exercise (*47*) and

in age-related tissue damage during aging (*18*). IFN-γ accumulation leads to mitochondrial defects, including swelling, impaired structural integrity, and loss of components required for energy production, such as electron transport chain complexes. Thus, muscle cells become metabolically compromised and cannot meet exercise-related energy demands. A well-documented function of T_{reg} cells is the control of IFN-γ production (*17*). Together, T_{reg} cells overexpressing Bcl-xL infiltration could be acting as shields preventing IFN-γ–mediated damage accumulation with aging, thereby promoting muscle mitochondria health and reducing frailty.

Bcl-xL maintains the muscle mitochondrial structure and function and prevents frailty

The role of mitochondria in aging is far more complicated than suggested by the mitochondrial free radical theory of aging. Several changes in mitochondrial ultrastructure, function, biogenesis, dynamics, and quality control (through mitophagy) contribute to aging and tissue dysfunction. Damaged mitochondria have a deregulated mitochondrial electron transport chain leading to inefficient OXPHOS metabolism, which increases oxidative stress and damage to molecules. This in turn affects muscle regenerative capacity by regulating satellite cell metabolism and proliferation during aging (*48*).

The aging phenotype is characterized by poor physical health because of low activity levels, reduced physical performance, and increased prevalence of frailty. This decline in physical function is associated with increased susceptibility to age-related diseases and reduced longevity in both rodents and humans (*49*).

Several studies have suggested a positive association between physical exercise and immune function. For instance, old-aged individuals who habitually practice physical exercise maintain an improved T cell function (e.g., increased levels of IL-2 and IL-4) compared to sedentary individuals of a similar age (*50*). Thus, given that Lck^{pr}-bcl-x_L mice overexpress Bcl-xL specifically in T cells, we believed that the improvement observed in these mice could be attributed to an enhanced T cell function (*21*).

A state of reduced physical activity will almost certainly evolve to frailty and, eventually, disability (*21*). Mice overexpressing Bcl-xL are less frail than controls, and hence, they display more successful aging. Reduced body weight in mice is associated with increased health span and lifespan (*51*, *52*). Our data revealed that mice overexpressing Bcl-xL in T cells were leaner, with lower body weights, which was due to a reduced accumulation of fat mass during aging. Increased fat tissue can contribute to metabolic diseases (*53*). We observed that wild-type animals displayed reduced glucose tolerance at older ages. The protection against age-related glucose intolerance observed in Bcl-xL mouse strain may be also attributed to a T cell–dependent regulation of pancreatic cells. Recent studies reported that dysfunctional T cells cause glucose intolerance accompanied by reduced insulin secretion and increased chronic inflammation in mice (*54*, *55*) and pigs (*56*).

In conclusion, the major aim of this work was to evaluate whether Bcl-xL, a gene that is specifically overexpressed in centenarians (*4*), promotes successful aging in mice phenocopying the observed increase of this protein in centenarian T cells. Mice overexpressing Bcl-xL in T cells, as they age, display improved T cell function and lower inflammation and maintain mitochondrial structure and function in muscle.

The significance of this study lies in the proposition of a molecular mechanism underlying the maintenance of vitality during successful aging, grounded in genetic discoveries among centenarians. This exemplifies reverse translation, wherein human findings serve to elucidate successful aging mechanisms by testing them in genetically modified animal models.

Here, we report findings on physical fitness promoted by Bcl-xL. Our aim in the immediate future will be to test the effect of Bcl-xL on cognition. This is led by the general idea that centenarians and their offspring not only delay the loss of physical fitness but may also maintain cognitive function. The long-term aim of our studies is to identify safe ways of promoting Bcl-xL expression in humans.

MATERIALS AND METHODS

Mouse model and care

In this study, we used heterozygous mice from the B6.Cg-Tg(LCKprBCL2L1)12Sjk/J (Lck^{pr}-bcl-x_L) strain purchased from the Jackson Laboratory (stock number 013738). These mice overexpress the human Bcl-xL cDNA sequence under the control of a mouse lymphocyte protein tyrosine kinase proximal promoter (*Lck*^{pr}). This promoter drives Bcl-xL expression in all thymocyte subsets. Mice were housed in the animal center of the Central Unit for Research in Medicine (UCIM) of the Faculty of Medicine and Odontology of the University of Valencia. Animals were kept in the facility at 22 ± 2°C, with a relative humidity of 60% under 12/12 hours of dark/light cycles and with access to food and water ad libitum. All the experiments performed with these animals have been approved by the Ethics Committee of the University of Valencia and by the Conselleria d'Agrigultura, Medi Ambient, Canvi Climàtic I Desenvolupament Rural of the Generalitat Valenciana (ID numbers 2021/VSC/PEA/0215 and 2022/VSC/PEA/0203).

Genotyping and colony formation

Two DNA sequences were amplified: one corresponding to the *BCL2L1* transgene (400 base pairs) and the internal positive control (200 base pairs), both purchased from the Jackson Laboratory. Sequences: BCL-XL forward (GCA TTC AGT GAC CTG ACA TC), BCL-XL reverse (CTG AAG AGT GAG CCC AGC AGA ACC), control forward (CAA ATG TTG CTT GTC TGG TG), and control reverse (GTC AGT CGA GTG CAC AGT TT). The tissue was digested with Kit Kapa following the manufacturer's instructions. The applied polymerase chain reaction program was as follows: 1× 2 min at 94°C, 10× (20 s at 94°C, 15 s at 65°C, and 10 s at 68°C), 28× (15 s at 94°C, 15 s at 60°C, and 10 s at 72°C), 1× 2 min at 72°C, and hold at 4°C. Then, 5 μl of each sample was loaded in agarose gels supplemented with tris-acetate-EDTA buffer and Red Safe solution. Electrophoresis was run at 100 V for 20 to 30 min. Images were obtained using the ImageQuant LAS 4000 camera system. Lck^{pr}-bcl-x_L transgenic mice were bred with C57BL/6J wild-type mice to establish the heterozygous colony.

Study design

We divided our mice into four age groups to study the effect of Bcl-xL overexpression during aging, considering 2- to 5-month-old mice as young, 8- to 11-month-old mice as adults, 17- to 20-month-old mice as old, and 24- to 26-month-old mice as very old. We established an initial cohort of Lck^{pr}-bcl-x_L and C57BL/6J mice, with females and males in similar proportions. When mice reached each age group respectively, body composition and physical performance assays were performed longitudinally. Animals were then euthanized by cervical dislocation. Blood samples were processed for plasma obtention and

stored at −80°C. For each mouse, half brain, cerebellum, heart, lungs, one gastrocnemius, liver, kidney, aorta, whole blood, and thymus were used fresh or freeze-clamped and stored at −80°C. In parallel, spleens were removed from mice for immediate fresh T cell isolation. The other gastrocnemius was removed and sliced: One slice was submerged in fixative buffer and stored at 4°C, and the rest of the tissue was processed for immediate fresh mitochondria isolation.

Body composition

Body weight

Three measurements of body weight were assessed on day 0 (before the physical performance assays), day 7 (on the first day of the assays), and day 14 (after the assays) using a precision balance. The mean was calculated for each mouse in each age group. Individual body weight gain was calculated as the percentage of increment with respect to the young age.

Body mass

Body mass composition was evaluated using the dual energy x-ray absorptiometry analyzer (Medikors Inc.) for laboratory animals. Mice were anesthetized with the isoflurane vaporizer before and during the measurement. Mice's total mass, fat mass, and lean mass were analyzed.

Glucose and insulin tolerance test

Glycemia was measured in blood drops from the saphenous vein before (0 min) and after (15, 30, 60, 120, and 180 min) the intraperitoneal injection of glucose (2 g/kg) in 12-hour fasted mice. The glucometer Accu-Check Guide Me and the corresponding test strips were used for this test.

Metabolic profiling

We determined the metabolic phenotype from 8- to 11- and 17- to 20-month-old mice by monitoring with the OxyletPro Physiocage (Panlab). This system integrates the evaluation of respiratory metabolism, food, and drink intake, as well as spontaneous locomotor activity that allows the determination of overall metabolic function in rodents. Mice were placed individually in the metabolic cages for ~45 hours.

Physical performance

Grip strength test

Mice's forelimb grip strength was measured using the dynamometer Grip Strength Test (BIOSEB). Each mouse was tested three times. This procedure was performed twice before the day of the test to ensure the adaptation of the animals to the evaluation process. Grip strength loss was calculated as the percentage of loss with respect to the young age.

Rotarod test

Motor coordination was determined using the Rotarod apparatus (Harvard Apparatus). The test was set at 4 to 40 rpm for 300 s. Each mouse was tested three times. This procedure is performed three times before the day of the test to ensure the adaptation of the animals to the evaluation process. Motor coordination loss was calculated as the percentage of latency time loss with respect to the young age.

Treadmill incremental test

Physical endurance was analyzed with the incremental treadmill test using the treadmill apparatus (Harvard Apparatus). The treadmill was set with an inclination angle of 2.86° (5%). Mice were allowed to run for 4 min at a constant velocity of 10 cm/s. Then, the speed was increased by 4 cm/s every 2 min until exhaustion. A 10-min acclimatization to the test is performed twice before the day of the assay to ensure adaptation of the animals to the treadmill apparatus. Physical endurance loss was calculated as the percentage of running time loss with respect to the young age.

Frailty assessment

To identify frail mice, we used a combination of the frailty criteria used by Bauman and colleagues (*57*) and a modified version of the Valencia score for frailty developed by our group (*22*). The mentioned criteria are based on the frailty score used in humans developed by Fried and collaborators (*58*) but adapted to experimental animals. We assessed frailty in 17- to 20- and 24- to 26-month-old mice using the frailty criteria and a cutoff value of 20%. According to the number of criteria met, mice were classified as frail (>2), prefrail (=2), and nonfrail (<2).

Muscle regeneration

To induce muscle injury in vivo, middle-aged mice received an injection of 4% $BaCl_2$ into the right gastrocnemius (15 μl), and the same volume of phosphate-buffered saline (PBS) was administered into the left gastrocnemius. Mice were kept warm during recovery and then returned to their cage. At days 4 and 10 postinjection, mice were euthanized, and muscle samples were collected in 4% paraformaldehyde (PFA).

Tissue homogenization

Freeze-clamped organs were homogenized using the Precellys Evolution homogenizer (Bertin Technologies). For each organ, 30 to 50 mg of tissue were mixed with the corresponding buffer at a 1/10 (w/v) proportion. Samples were processed using a pre-set protocol (6800 rpm, 4°C, and three cycles of 20 s each) by the manufacturer. Homogenates were then centrifuged at 1500*g* for 5 min at 4°C, and supernatants were sonicated by four pulses at 36% amplitude using a VCX 740 Sonicator.

Protein quantification

Total protein was quantified using either the Lowry-Folin (*59*) or Bradford method (*60*) according to the sample's buffer compatibility. In both cases, total protein was calculated using a bovine serum albumin (BSA) standard curve (Panreac). Absorbances were measured using a spectrophotometer (Jenway) at 660 or 595 nm for the Lowry-Folin method or Bradford method, respectively.

Western blot

Tissues and cells were homogenized in lysis buffer (tris/SDS/glycerol buffer supplemented with a cocktail of protease and phosphatase inhibitors). Thirty micrograms of total protein was separated on SDS polyacrylamide gels and transferred onto polyvinylidene difluoride membranes. The membranes were blocked with 5% BSA in tris-buffered saline and 0.1% Tween 20 (TBS-T) for 60 min at room temperature (RT) and incubated overnight at 4°C with primary antibodies. Following three washes (10 min) with TBS-T, membranes were incubated with secondary antibodies for 60 min at RT. After three washes with TBS-T, membranes were developed with Luminol (Sigma-Aldrich) in an ImageQuant LAS4000 system. Images were processed in ImageJ. Primary antibodies: BCL-XL (Cell Signaling, no. 2762S), p53 (Cell Signaling, no. 9284S), γH2AX (Cell Signaling, no. 9718S), cytochrome c (Santa Cruz, sc-13156), caspase 9 (Cell Signaling, no. 9508), LC3-II (Cell Signaling, no. 3868S), TFAM (transcription factor A, mitochondrial; Proteintech, 22586-1-AP), and GAPDH

(glyceraldehyde-3-phosphate dehydrogenase; Sigma-Aldrich, G9545). Secondary antibodies: anti-rabbit immunoglobulin G (IgG; Cell Signaling, no. 7074S) and anti-mouse (Sigma-Aldrich, 401215).

Protein carbonylation

Tissues were homogenized in lysis buffer together with a reducing agent (50 mM dithiothreitol). Twenty micrograms of total protein was subjected to derivatization using the Oxyblot Protein Oxidation Detection Kit (Merck Millipore) following the manufacturer's instructions. The resulting protein mixture was separated on SDS polyacrylamide gels and transferred onto nitrocellulose membranes. The membranes were blocked with 1% BSA in PBS and 0.05% Tween 20 (PBS-T) for 60 min at RT and incubated overnight at 4°C with a primary antibody (1:150 in blocking solution). Following three washes (10 min) with PBS-T, membranes were incubated with a secondary antibody (1:300 in blocking solution) for 3 hours at RT. After three washes with PBS-T membranes, they were developed with Luminol (Sigma) in an ImageQuant LAS4000 system. Images were processed in ImageJ. Ponceau staining of the membranes was used as loading control.

Lipid peroxidation

Tissues were homogenized with a KPi-EDTA buffer (50 mM KPi and 1 mM EDTA, pH 7.4). Lipid peroxidation was assessed as MDA levels, which were detected using ultraperformance liquid chromatography as an MDA-thiobarbituric acid (TBA) adduct. This adduct ($MDA\text{-}TBA_2$) was detected using ultraperformance liquid chromatography in reverse phase and quantified at 532 nm. The chromatographic technique was performed under isocratic conditions (25% phase A + 75% phase B), where mobile phase A is acetonitrile and mobile phase B is a mixture of water + 0.3% phosphoric acid. The temperature column was set at 30°C and the flux at 0.2 ml/min. Levels of MDA in each sample were correlated to the concentration of total protein.

Cell lines and culture

To study how Bcl-xL is degraded, we used mouse embryonic fibroblasts (MEFs) and NIH3T3 mouse fibroblasts purchased from American Type Culture Collection and cultured in high-glucose Dulbecco's modified Eagle's medium (DMEM) with 1% penicillin/streptomycin (P/S) (Life Technologies). MEFs were cultured with or without 10% fetal bovine serum (FBS) for autophagy induction and treated with or without 20 mM NH_4Cl + 100 μM leupeptin (N/L) for lysosomal activity inhibition during 24 hours. At 6, 12, and 24 hours, MEFs were harvested for protein analysis by Western blot.

To study the effect of Bcl-xL overexpression on autophagy, we used the 293T packaging cell line, which was purchased from American Type Culture Collection and cultured in high-glucose Dulbecco's modified Eagle's medium with 10% FBS (both from Life Technologies). 293T cells were cotransfected with the Bcl-xL expression vector pCDH-puro-BCL-XL (plasmid no. 46972) or control vector pLKO.1-puro (plasmid no. 8453) (both from Addgene) along with the lentiviral packing plasmids ENV VSV-G, REV, and pMDLg/pRRR (III generation packing), as described before (*61*). After 48 hours, the medium containing lentivirus was collected. Then, NIH3T3 cells were transduced with lentivirus that contained the vector pCDH-puro-BCL-XL or control vector pLKO.1-puro. On day 3 after transduction, cells were cultured in the presence of puromycin (0.5 μg/ml) for 14 days to select stable Bcl-xL–overexpressing cells. The Bcl-xL–overexpressing and control cells were harvested for Bcl-xL protein analysis by Western blot.

Macroautophagy reporter

To evaluate the Bcl-xL effect on macroautophagy, NIH3T3 cells stably expressing Bcl-xL or pLKO control vector were also transfected with the macroautophagy reporter (mCherry-GFP-LC3) overnight (*62*). Imaging of the mCherry-GFP-LC3 reporter shows the fluorescence difference between autophagosomes (mCherry-GFP–positive puncta) and autolysosomes (mCherry only–positive puncta) in a cell. Adherent NIH3T3 cells (Bcl-xL–overexpressing and vector control) were grown on sterile coverslips in the bottom of 24-well plates with or without FBS to induce starving conditions. Once semiconfluent, cells were fixed with 3% formaldehyde at 37°C for 5 min and then at RT for 25 min. Cells were washed with PBS, and with the help of forceps, the coverslips were removed from the well plates and placed upside down on slides with one drop of 4′,6-diamidino-2-phenylindole (DAPI) fluoromount-G (Thermo Fisher Scientific). Cells were analyzed using an Axiovert 200 inverted fluorescence microscope (Zeiss).

Splenic T cells

Fresh spleens were mashed using the plunger of a 10-ml syringe with 1 ml of red blood cell lysis buffer (BD Pharm Lyse). The mixture was filtered through a 70-μm cell strainer and incubated for 10 min at RT. Then, mixtures were centrifuged at 300*g* for 10 min at RT. Supernatants were processed with the EasySep Mouse T Cell Isolation Kit (Stemcell Technologies), which isolates T cells from single-cell suspensions of splenocytes by negative selection. Unwanted cells are targeted for removal with biotinylated antibodies directed against non-T cells and streptavidin-coated magnetic particles. Labeled cells are separated using an EasySep magnet (Stemcell Technologies). Desired cells are poured off into a new tube and centrifuged at 180*g* for 5 min at RT. Pellets were resuspended in 1 ml of recommended medium (RM; PBS, 2% FBS, and 1 mM EDTA), 10 μl of each sample was introduced in a chamber slide (Bio-Rad), and T cells were counted in an Automated Cell Counter (Bio-Rad).

Splenic T cell culture

For the experiments that required cell culture, 1 million freshly isolated T cells were seeded per p12-well plate with 0.5 ml of RPMI 1640 medium (Gibco) supplemented with glutamine, 1% P/S, and 10% FBS in a heat gas incubator at 5% CO_2. For the study of apoptosis in cultured cells, T cells were seeded without FBS or treated with 100 nM dexamethasone (Sigma-Aldrich) for 12, 24, and 48 hours. For the study of cytokine production, T cells were seeded in p24-well plates at a density of 500,000 cells per well with 0.5 ml of RPMI 1640 + 10% FBS + 1% P/S and stimulated with 1× PMA + ionomycin (eBioscience Cell Stimulation Cocktail, ref. 00-4970-93) for 24 hours.

Enzyme-linked inmunosorbent analysis (ELISA)

IFN-γ levels in plasma samples were measured by an enzyme-linked inmunosorbent analysis (ELISA) kit (Thermo Fisher Scientific, no. KMC4021). TNFα, IL-6, IL-1β, and IFN-γ levels in T cell supernatants were also measured by ELISA kits (RayBiotech; refs. ELM-TNFa-1, ELM-IL6-1, ELM-IL1b-1, and ELM-IFNg-1). Sample preparation, processing, and detection were performed according to the manufacturer's instructions.

Flow cytometry analysis

To evaluate the efficiency of the T cell isolation protocol, we added 5 µl of APC anti-mouse CD3ε (BioLegend) to aliquots with 0.5 million T cells suspended in 200 µl of RM. After a 10-min incubation in the dark at 37°C, the volume was adjusted to 500 µl with cold RM.

To assess cultured T cell apoptosis, we used the annexin V kit (Immunostep). Briefly, we added 5 µl of CF-Blue Annexin V to aliquots with 0.5 million T cells suspended in 100 µl of RM + 100 µl of binding buffer. After a 10-min incubation in the dark at 37°C, the volume was adjusted to 500 µl with cold binding buffer supplemented with propidium iodide (1:100).

To determine the evolution of the different T cell populations, we used the mouse naïve/effector/memory kit (Cell Signaling, no. 78148), which includes the following antibodies: CD3 (PE), CD4 (violetFluor 450), CD8α (PE-Cy7), CD44 (PE-Cy5), CD62L/L-Selectin (FITC), and CD127/IL-7Rα (APC). The gating strategy for observing naïve, effector, and memory T cell subsets was as follows: First, the gate on lymphocytes was based on forward scatter and side scatter. T helper cells are the $CD3^+$ $CD4^+$ cells within the lymphocyte gate. Cytotoxic T cells are the $CD3^+$ $CD8^+$ cells within the lymphocyte gate. Next, the expression of CD44 versus CD62L was observed on either T helper cells or cytotoxic T cells. Naïve T cells are $CD44^-$ $CD62L^+$. Central memory T cells are $CD44^+$ $CD62L^+$. Effector memory and effector cells are $CD44^+$ $CD62L^-$. To distinguish effector memory and effector cells, observe the expression of CD127/IL-7Rα on the $CD44^+$ $CD62L^-$ population. Effector memory cells are positive for the expression of CD127/IL-7Rα. Effector cells are negative for the expression of CD127/IL-7Rα. Naïve and central memory T cells also express CD127/IL-7Rα.

To assess T_{reg} levels in whole blood and in lymphoid tissues (spleen), both samples were processed with the BD Pharmingen FoxP3 Buffer set (BD Biosciences, no. 560098) for the fixation and permeabilization before surface staining with FITC anti-mouse CD4 (Elabscience, E-AB-F1097C) and APC anti-mouse CD25 (Elabscience, E-AB-F1102E) and intracellular staining with PE anti-mouse FoxP3 (Elabscience, E-AB-F1238D) following the manufacturer's instructions. All samples were analyzed using a FACS-Verse flow cytometer (BD Biosciences, San Diego, CA) until 100,000 events were recorded.

Seahorse

An XFe96 extracellular flux analyzer (Seahorse Bioscience, Agilent Technologies) was used to measure OCR and ECAR (extracellular acidification rate). The day before the assay, the XFe Sensor Cartridge was hydrated using XFe Calibrant at 37°C in a non-CO_2 incubator overnight. A total of 500,000 T cells was seeded into each well of a 96 XFe Cell Culture Microplate with 180 µl of unbuffered XFe Base Medium (pH 7.4) supplemented with 1 mM pyruvate, 2 mM glutamine, and 10 mM glucose. The XFe Cell Mito Stress Test consists of sequential compound injections of 1 µM oligomycin, 2 µM FCCP, and a 0.5 µM mix of rotenone/antimycin A. This kit measures key parameters of mitochondrial function such as ATP production, maximal respiration, and nonmitochondrial respiration, respectively. Proton leak and spare respiratory capacity were then calculated using these parameters and basal respiration.

Immunofluorescence analysis

Nonadherent splenic T cells (wild-type and transgenic) were cultured in the presence or absence of FBS to induce starving conditions. After 4 hours of culture, at the peak of macroautophagy activation, cells were permeabilized using the Anti-Human/Mouse INTRACELL kit (INTRA-100 Immunostep) according to the manufacturer's instructions. Cells were stained with 100 µl of LC3B in PBS and 1% BSA and incubated overnight at 4°C in the dark. Cells were washed with PBS and stained with 100 µl of Alexa Fluor 488 anti-rabbit IgG in PBS and 1% BSA for 1 hour at RT in the dark. The volume was adjusted to 500 µl with a flow cytometry buffer. Nonadherent T cells were analyzed using a FACS-Verse flow cytometer (BD Biosciences, San Diego, CA) until 100,000 events were recorded.

Adherent NIH3T3 cells (Bcl-xL–overexpressing and vector control) were grown on sterile coverslips in the bottom of 24-well plates. Once semiconfluent, the medium was removed and replaced with a pre-warmed probe-containing medium (50 nM LysoTracker). Cells were incubated for 30 min at 37°C. Then, the media were replaced with a fresh medium, and with the help of forceps, the coverslips were removed from the well plates and placed upside down on slides with one drop of DAPI fluoromount-G (Thermo Fisher Scientific). Cells were analyzed using an Axiovert 200 inverted fluorescence microscope (Zeiss).

Adherent NIH3T3 cells (Bcl-xL–overexpressing and vector control) were grown on sterile coverslips in the bottom of 24-well plates. Once semiconfluent, cells were fixed with 3% formaldehyde at 37°C for 5 min and then at RT for 25 min. Cells were washed with PBS and incubated with a blocking solution for 30 min at RT. Cells were washed with PBS and stained with a primary antibody in 100 µl of PBS and 0.1% BSA and incubated overnight at 4°C in the dark. Cells were washed with PBS and stained with 100 µl of secondary antibody in PBS and 0.1% BSA for 1 hour at RT in the dark. Cells were washed with PBS, and with the help of forceps, the coverslips were removed from the well plates and placed upside down on slides with one drop of DAPI fluoromount-G (Thermo Fisher Scientific) and sealed with nail polish. Cells were analyzed using an Axiovert 200 inverted fluorescence microscope (Zeiss).

Gastrocnemius samples were fixed in 4% PFA for 48 hours and then cryoprotected with 30% sucrose in PBS; 10-µm slices were obtained using a cryostat for histological staining and immunofluorescence. The 10-µm slices were mounted in slides and heated for 30 min in tris-EDTA buffer (pH 10) for antigen retrieval and permeabilized with 1% Triton X-100 in PBS or 1% Tween 20 in PBS. Sections were blocked with 10% normal goat serum (Invitrogen) in PBS-T and incubated with a primary antibody overnight at 4°C. After incubation with a primary antibody, sections were washed three times with PBS-T and incubated with a secondary antibody for 2 hours at RT. Washes were repeated, and coverslips were mounted with one drop of DAPI fluoromount-G (Thermo Fisher Scientific) and sealed with nail polish. Images were acquired with an Olympus FV1000 confocal laser scanning biological microscope. Images were processed in ImageJ, all levels were adjusted equally, the ratios were not altered, and three images from different areas of each slice were obtained. A minimum of 500 nuclei was analyzed per sample.

Primary antibodies: LC3B (Cell Signaling, no. 3868S) and LAMP1 (Enzo, ADI-VAM-EN001), CD3 (Proteintech, 17617-1-AP), FoxP3 (Proteintech, 65089-1-Ig), and α-tubulin (Proteintech, 11224-1-AP). Secondary antibodies: Alexa Fluor 488 anti-rabbit IgG (Abcam, ab150077), Alexa Fluor 647 anti-mouse IgG (Cell Signaling, no. 4410S), and cyanine 5 anti-mouse (Abcam, ab6563).

Histological analysis

Slices (10 µm) were obtained using a cryostat for histological staining and immunofluorescence. Slices were stained with hematoxylin

(Sigma-Aldrich, MHS32) and eosin (Sigma-Aldrich, E4009) and mounted and sealed for morphometric analysis. Images were obtained using an optical microscope (Leica), and three images from different areas of each slice were obtained. A minimum of 200 fibers was analyzed per sample. All levels were adjusted equally, the ratios were not altered, and morphometric analysis of muscle sections was performed with ImageJ.

Mitochondria from gastrocnemius muscle

One hundred milligrams of fresh gastrocnemius muscle tissue (freed from collagen and nerves) was placed in an Eppendorf tube with 1 ml of PBS + 10 mM EDTA (pH 7.4) on ice. The medium was removed, and the tissue was mechanically digested using scissors. One milliliter of cold disaggregation buffer (PBS + 0.05% trypsin + 10 mM EDTA) was added and incubated for 30 min in a rotating wheel at 4°C. It was centrifuged at 350*g* for 5 min at 4°C. The supernatant was discarded, and the pellet was resuspended in 1.5 ml of PBS + 10 mM EDTA. It was centrifuged again at 350*g* for 5 min at 4°C. The supernatant was removed, and the pellet was resuspended in 3 ml of Freeza medium [67 mM sucrose + 50 mM KCl + 50 mM tris-HCl + 10 mM EDTA + BSA (1 mg/ml)]. The sample (10 fast strokes followed by 10 slow strokes) was homogenized mechanically using a Potter-Elvehjem homogenizer consisting of a large clearance Teflon pestle driven into a glass vessel (volume, 2 ml) connected to an Ultra-Turrax dispersor. It was centrifuged at 1000*g* for 5 min at 4°C. The supernatant was placed in a new Eppendorf tube and centrifuged at 10,000*g* for 5 min at 4°C. The pellet containing mitochondria was resuspended with 500 μl of Freeza medium and kept on ice until use.

Transmission electron microscopy

Fresh gastrocnemius muscle tissue was sliced with a scalpel and immersed in Karnovsky fixative solution (supplemented with 2.5% PFA and 2.5% glutaraldehyde) for 2 hours at 4°C. Further, it was fixed with 1% osmium tetroxide for 1.5 hours and then dehydrated in alcohol series with increasing alcohol concentrations of 50, 60, 70, 80, and 96% (70% alcohol contained 1.4% uranyl acetate) to enhance contrast. After that, samples were embedded in epoxy resin. A series of ultrathin sections was prepared with an ultramicrotome (Leica) and stained with lead. The obtained preparations were imaged and photographed under a TEM HITACHI HT7800 transmission electron microscope (HITACHI High-Tech Corporation) operating at the accelerating voltage of 120 kV equipped with a CMOS EMSIS XAROSA camera.

Oroboros

An Oroboros O2k-FluoRespirometer (Oroboros Instruments) was used to assess high-resolution respirometry that allows simultaneous monitoring of oxygen consumption and oxygen flux. Before each test, cleaning before the protocol was performed followed by an air calibration setup. Both chambers were filled with 2 ml of MIR05 medium and 50 μg of freshly isolated mitochondria from muscle. Then, the SUIT20 procedure was applied to each sample, which consisted of serial injections of 2 M pyruvate (fresh), 400 mM malate, 500 mM adenosine 5′-diphosphate, 4 mM cytochrome c, 2 M glutamate, 1 M succinate, 1 mM rotenone, oligomycin (4 mg/ml), 1 mM FCCP, and 5 mM antimycin A following the manufacturer's instructions. At the end of each experiment, cleaning after protocol was performed.

Statistical analysis

Statistical data were obtained with Excel (Microsoft 365 Family), and low-throughput statistical analysis was performed using GraphPad Prism (version 9.5.0). All data are presented as the means ± SD, and a P value of <0.05 was considered statistically significant. Different statistical tests were performed depending on the variable type (numerical or categorical) and whether the data met the assumptions of the parametric tests. For numerical variables, the two-sample Student's t test and the analysis of variance (ANOVA) F test were used when sampling distributions displayed normal residuals and the population variances were identical, which is generally known as the homoscedasticity assumption. For categorical variables, such as the frailty group, we created a contingency table and performed Fisher's exact test.

REFERENCES AND NOTES

1. K. Ismail, L. Nussbaum, P. Sebastiani, S. Andersen, T. Perls, N. Barzilai, S. Milman, Compression of morbidity is observed across cohorts with exceptional longevity. *J. Am. Geriatr. Soc.* **64**, 1583–1591 (2016).
2. F. Sierra, R. Kohanski, Geroscience and the trans-NIH Geroscience Interest Group, GSIG. *Geroscience* **39**, 1–5 (2017).
3. G. Pawelec, M. Adibzadeh, H. Pohla, K. Schaudt, Immunosenescence: Ageing of the immune system. *Immunol. Today* **16**, 420–422 (1995).
4. C. Borras, K. M. Abdelaziz, J. Gambini, E. Serna, M. Ingles, M. de la Fuente, I. Garcia, A. Matheu, P. Sanchis, A. Belenguer, A. Errigo, J. A. Avellana, A. Barettino, C. Lloret-Fernandez, N. Flames, G. Pes, L. Rodriguez-Manas, J. Vina, Human exceptional longevity: Transcriptome from centenarians is distinct from septuagenarians and reveals a role of Bcl-xL in successful aging. *Aging* **8**, 3185–3208 (2016).
5. C. Borrás, C. Mas-Bargues, A. Román-Domínguez, J. Sanz-Ros, L. Gimeno-Mallench, M. Inglés, J. Gambini, J. Viña, BCL-xL, a mitochondrial protein involved in successful aging: From C. elegans to human centenarians. *Int. J. Mol. Sci.* **21**, 418 (2020).
6. C. Mas-Bargues, C. Borrás, J. Viña, Bcl-xL as a modulator of senescence and aging. *Int. J. Mol. Sci.* **22**, 1527 (2021).
7. C. Franceschi, A. Santoro, M. Capri, The complex relationship between Immunosenescence and Inflammaging: Special issue on the New Biomedical Perspectives. *Semin. Immunopathol.* **42**, 517–520 (2020).
8. H. E. Kunz, I. R. Lanza, Age-associated inflammation and implications for skeletal muscle responses to exercise. *Exp. Gerontol.* **177**, 112177 (2023).
9. D. Wilson, T. Jackson, E. Sapey, J. M. Lord, Frailty and sarcopenia: The potential role of an aged immune system. *Ageing Res. Rev.* **36**, 1–10 (2017).
10. D. A. Hood, J. M. Memme, A. N. Oliveira, M. Triolo, Maintenance of skeletal muscle mitochondria in health, exercise, and aging. *Annu. Rev. Physiol.* **81**, 19–41 (2019).
11. X. Xu, Z. Wen, The mediating role of inflammaging between mitochondrial dysfunction and sarcopenia in aging: A review. *Am. J. Clin. Exp. Immunol.* **12**, 109–126 (2023).
12. S. Aggarwal, S. Gupta, Increased apoptosis of T cell subsets in aging humans: Altered expression of Fas (CD95), Fas ligand, Bcl-2, and Bax. *J. Immunol.* **160**, 1627–1637 (1998).
13. C. L. Montes, B. A. Maletto, E. V. Acosta Rodriguez, A. Gruppi, M. C. Pistoresi-Palencia, B cells from aged mice exhibit reduced apoptosis upon B-cell antigen receptor stimulation and differential ability to up-regulate survival signals. *Clin. Exp. Immunol.* **143**, 30–40 (2006).
14. T. W. Behrens, D. L. Mueller, Bcl-x and the regulation of survival in the immune system. *Immunol. Res.* **16**, 149–160 (1997).
15. J. Saini, J. S. McPhee, S. Al-Dabbagh, C. E. Stewart, N. Al-Shanti, Regenerative function of immune system: Modulation of muscle stem cells. *Ageing Res. Rev.* **27**, 67–76 (2016).
16. W. Kuswanto, D. Burzyn, M. Panduro, K. K. Wang, Y. C. Jang, A. J. Wagers, C. Benoist, D. Mathis, Poor repair of skeletal muscle in aging mice reflects a defect in local, interleukin-33-dependent accumulation of regulatory T cells. *Immunity* **44**, 355–367 (2016).
17. J. Larkin III, C. M. Ahmed, T. D. Wilson, H. M. Johnson, Regulation of interferon gamma signaling by suppressors of cytokine signaling and regulatory T cells. *Front. Immunol.* **4**, 469 (2013).
18. W. Cao, IFN-aging: Coupling aging with interferon response. *Front. Aging Neurosci.* **3**, 870489 (2022).
19. J. A. Amorim, G. Coppotelli, A. P. Rolo, C. M. Palmeira, J. M. Ross, D. A. Sinclair, Mitochondrial and metabolic dysfunction in ageing and age-related diseases. *Nat. Rev. Endocrinol.* **18**, 243–258 (2022).
20. S. Cogliati, C. Frezza, M. E. Soriano, T. Varanita, R. Quintana-Cabrera, M. Corrado, S. Cipolat, V. Costa, A. Casarin, L. C. Gomes, E. Perales-Clemente, L. Salviati, P. Fernandez-Silva,

J. A. Enriquez, L. Scorrano, Mitochondrial cristae shape determines respiratory chain supercomplexes assembly and respiratory efficiency. *Cell* **155**, 160–171 (2013).
21. A. Román-Domínguez, "Study of the role of BCL-XL in healthy aging and frailty prevention," thesis, University of Valencia (2023).
22. M. C. Gomez-Cabrera, R. Garcia-Valles, L. Rodriguez-Mañas, F. J. Garcia-Garcia, G. Olaso-Gonzalez, A. Salvador-Pascual, F. J. Tarazona-Santabalbina, J. Viña, A new frailty score for experimental animals based on the clinical phenotype: Inactivity as a model of frailty. *J. Gerontol. A Biol. Sci. Med. Sci.* **72**, 885–891 (2017).
23. I. de Martinez Toda, A. Garrido, C. Vida, M. C. Gomez-Cabrera, J. Vina, M. De la Fuente, Frailty quantified by the "Valencia Score" as a potential predictor of lifespan in mice. *J. Gerontol. A Biol. Sci. Med. Sci.* **73**, 1323–1329 (2018).
24. K. N. Alavian, H. Li, L. Collis, L. Bonanni, L. Zeng, S. Sacchetti, E. Lazrove, P. Nabili, B. Flaherty, M. Graham, Y. Chen, S. M. Messerli, M. A. Mariggio, C. Rahner, E. McNay, G. C. Shore, P. J. Smith, J. M. Hardwick, E. A. Jonas, Bcl-xL regulates metabolic efficiency of neurons through interaction with the mitochondrial F1FO ATP synthase. *Nat. Cell Biol.* **13**, 1224–1233 (2011).
25. M. Mittelbrunn, G. Kroemer, Hallmarks of T cell aging. *Nat. Immunol.* **22**, 687–698 (2021).
26. C. Mas-Bargues, Mitochondria pleiotropism in stem cell senescence: Mechanisms and therapeutic approaches. *Free Radic. Biol. Med.* **208**, 657–671 (2023).
27. L. H. Boise, A. J. Minn, P. J. Noel, C. H. June, M. A. Accavitti, T. Lindsten, C. B. Thompson, CD28 costimulation can promote T cell survival by enhancing the expression of Bcl-XL. *Immunity* **3**, 87–98 (1995).
28. L. H. Boise, A. J. Minn, P. J. Noel, C. H. June, M. A. Accavitti, T. Lindsten, C. B. Thompson, CD28 costimulation can promote T cell survival by enhancing the expression of Bcl-xL. Immunity. 1995. 3: 87–98. *J. Immunol.* **185**, 3788–3799 (2010).
29. T. H. Watts, Staying alive: T cell costimulation, CD28, and Bcl-x_L. *J. Immunol.* **185**, 3785–3787 (2010).
30. A. M. Cuervo, E. Bergamini, U. T. Brunk, W. Dröge, M. Ffrench, A. Terman, Autophagy and aging: The importance of maintaining "clean" cells. *Autophagy* **1**, 131–140 (2005).
31. Y. Raz, I. Guerrero-Ros, A. Maier, P. E. Slagboom, G. Atzmon, N. Barzilai, F. Macian, Activation-induced autophagy is preserved in CD4+ T-cells in familial longevity. *J. Gerontol. A Biol. Sci. Med. Sci.* **72**, 1201–1206 (2017).
32. P. Sansoni, R. Vescovini, F. Fagnoni, C. Biasini, F. Zanni, L. Zanlari, A. Telera, G. Lucchini, G. Passeri, D. Monti, C. Franceschi, M. Passeri, The immune system in extreme longevity. *Exp. Gerontol.* **43**, 61–65 (2008).
33. M. Pinti, M. Nasi, E. Lugli, L. Gibellini, L. Bertoncelli, E. Roat, S. De Biasi, C. Mussini, A. Cossarizza, T cell homeostasis in centenarians: From the thymus to the periphery. *Curr. Pharm. Des.* **16**, 597–603 (2010).
34. E. Derhovanessian, A. B. Maier, R. Beck, G. Jahn, K. Hahnel, P. E. Slagboom, A. J. de Craen, R. G. Westendorp, G. Pawelec, Hallmark features of immunosenescence are absent in familial longevity. *J. Immunol.* **185**, 4618–4624 (2010).
35. M. Pellicano, S. Buffa, D. Goldeck, M. Bulati, A. Martorana, C. Caruso, G. Colonna-Romano, G. Pawelec, Evidence for less marked potential signs of T-cell immunosenescence in centenarian offspring than in the general age-matched population. *J. Gerontol. A Biol. Sci. Med. Sci.* **69**, 495–504 (2014).
36. A. Santoro, A. Bazzocchi, G. Guidarelli, R. Ostan, E. Giampieri, D. Mercatelli, M. Scurti, A. Berendsen, O. Surala, A. Jennings, N. Meunier, E. Caumon, R. Gillings, F. Kadi, F. Capel, K. D. Cashman, B. Pietruszka, E. J. M. Feskens, L. C. P. G. M. De Groot, G. Battista, S. Salvioli, C. Franceschi, A cross-sectional analysis of body composition among healthy elderly from the European NU-AGE Study: Sex and country specific features. *Front. Physiol.* **9**, 1693 (2018).
37. L. A. Callender, E. C. Carroll, R. W. J. Beal, E. S. Chambers, S. Nourshargh, A. N. Akbar, S. M. Henson, Human $CD8^+$ EMRA T cells display a senescence-associated secretory phenotype regulated by p38 MAPK. *Aging Cell* **17**, e12675 (2018).
38. S. M. Henson, N. E. Riddell, A. N. Akbar, Properties of end-stage human T cells defined by CD45RA re-expression. *Curr. Opin. Immunol.* **24**, 476–481 (2012).
39. C. H. Kim, FOXP3 and its role in the immune system. *Adv. Exp. Med. Biol.* **665**, 17–29 (2009).
40. D. Burzyn, W. Kuswanto, D. Kolodin, J. L. Shadrach, M. Cerletti, Y. Jang, E. Sefik, T. G. Tan, A. J. Wagers, C. Benoist, D. Mathis, A special population of regulatory T cells potentiates muscle repair. *Cell* **155**, 1282–1295 (2013).
41. S. Schiaffino, M. G. Pereira, S. Ciciliot, P. Rovere-Querini, Regulatory T cells and skeletal muscle regeneration. *FEBS J.* **284**, 517–524 (2017).
42. J. Weirather, U. D. Hofmann, N. Beyersdorf, G. C. Ramos, B. Vogel, A. Frey, G. Ertl, T. Kerkau, S. Frantz, Foxp3+ CD4+ T cells improve healing after myocardial infarction by modulating monocyte/macrophage differentiation. *Circ. Res.* **115**, 55–67 (2014).
43. A. Castiglioni, G. Corna, E. Rigamonti, V. Basso, M. Vezzoli, A. Monno, A. E. Almada, A. Mondino, A. J. Wagers, A. A. Manfredi, P. Rovere-Querini, FOXP3+ T cells recruited to sites of sterile skeletal muscle injury regulate the fate of satellite cells and guide effective tissue regeneration. *PLOS ONE* **10**, e0128094 (2015).
44. S. A. Villalta, W. Rosenthal, L. Martinez, A. Kaur, T. Sparwasser, J. G. Tidball, M. Margeta, M. J. Spencer, J. A. Bluestone, Regulatory T cells suppress muscle inflammation and injury in muscular dystrophy. *Sci. Transl. Med.* **6**, 258ra142 (2014).
45. J. Li, J. Tan, M. M. Martino, K. O. Lui, Regulatory T-cells: Potential regulator of tissue repair and regeneration. *Front. Immunol.* **9**, 585 (2018).
46. Z. Chen, H. Lan, Z. Liao, J. Huang, X. Jian, J. Hu, H. Liao, Regulatory T cells-centered regulatory networks of skeletal muscle inflammation and regeneration. *Cell Biosci.* **12**, 112 (2022).
47. P. K. Langston, Y. Sun, B. A. Ryback, A. L. Mueller, B. M. Spiegelman, C. Benoist, D. Mathis, Regulatory T cells shield muscle mitochondria from interferon-γ-mediated damage to promote the beneficial effects of exercise. *Sci. Immunol.* **8**, eadi5377 (2023).
48. X. Hong, J. Isern, S. Campanario, E. Perdiguero, I. Ramirez-Pardo, J. Segales, P. Hernansanz-Agustin, A. Curtabbi, O. Deryagin, A. Pollan, J. A. Gonzalez-Reyes, J. M. Villalba, M. Sandri, A. L. Serrano, J. A. Enriquez, P. Munoz-Canoves, Mitochondrial dynamics maintain muscle stem cell regenerative competence throughout adult life by regulating metabolism and mitophagy. *Cell Stem Cell* **29**, 1298–1314.e10 (2022).
49. C. D. Reimers, G. Knapp, A. K. Reimers, Does physical activity increase life expectancy? A review of the literature. *J. Aging Res.* **2012**, 243958 (2012).
50. T. Donovan, A. L. Bain, W. Tu, D. B. Pyne, S. Rao, Influence of exercise on exhausted and senescent T cells: A systematic review. *Front. Physiol.* **12**, 668327 (2021).
51. R. A. Miller, J. M. Harper, A. Galecki, D. T. Burke, Big mice die young: Early life body weight predicts longevity in genetically heterogeneous mice. *Aging Cell* **1**, 22–29 (2002).
52. C. W. Baumann, D. Kwak, L. V. Thompson, Sex-specific components of frailty in C57BL/6 mice. *Aging* **11**, 5206–5214 (2019).
53. R. Ostan, L. Bucci, E. Cevenini, M. G. Palmas, E. Pini, M. Scurti, R. Vescovini, C. Caruso, D. Mari, G. Vitale, C. Franceschi, D. Monti, Metabolic syndrome in the offspring of centenarians: Focus on prevalence, components, and adipokines. *Age* **35**, 1995–2007 (2013).
54. J. Sbierski-Kind, D. Goldeck, N. Buchmann, J. Spranger, H.-D. Volk, E. Steinhagen-Thiessen, G. Pawelec, I. Demuth, D. Spira, T cell phenotypes associated with insulin resistance: Results from the Berlin Aging Study II. *Immun. Ageing* **17**, 40 (2020).
55. E. Xu, M. M. A. Pereira, I. Karakasilioti, S. Theurich, M. Al-Maarri, G. Rappl, A. Waisman, F. T. Wunderlich, J. C. Bruning, Temporal and tissue-specific requirements for T-lymphocyte IL-6 signalling in obesity-associated inflammation and insulin resistance. *Nat. Commun.* **8**, 14803 (2017).
56. K. Zhang, C. Tao, J. Xu, J. Ruan, J. Xia, W. Zhu, L. Xin, H. Ye, N. Xie, B. Xia, C. Li, T. Wu, Y. Wang, M. Schroyen, X. Xiao, J. Fan, S. Yang, $CD8^+$ T cells involved in metabolic inflammation in visceral adipose tissue and liver of transgenic pigs. *Front. Immunol.* **12**, 690069 (2021).
57. C. W. Baumann, D. Kwak, L. V. Thompson, Assessing onset, prevalence and survival in mice using a frailty phenotype. *Aging* **10**, 4042–4053 (2018).
58. L. P. Fried, C. M. Tangen, J. Walston, A. B. Newman, C. Hirsch, J. Gottdiener, T. Seeman, R. Tracy, W. J. Kop, G. Burke, M. A. McBurnie, Frailty in older adults: Evidence for a phenotype. *J. Gerontol. A Biol. Sci. Med. Sci.* **56**, M146–M157 (2001).
59. O. H. Lowry, N. J. Rosebrough, A. L. Farr, R. J. Randall, Protein measurement with the Folin phenol reagent. *J. Biol. Chem.* **193**, 265–275 (1951).
60. M. M. Bradford, A rapid and sensitive method for the quantitation of microgram quantities of protein utilizing the principle of protein-dye binding. *Anal. Biochem.* **72**, 248–254 (1976).
61. A. C. Massey, S. Kaushik, G. Sovak, R. Kiffin, A. M. Cuervo, Consequences of the selective blockage of chaperone-mediated autophagy. *Proc. Natl. Acad. Sci. U.S.A.* **103**, 5805–5810 (2006).
62. S. Kimura, T. Noda, T. Yoshimori, Dissection of the autophagosome maturation process by a novel reporter protein, tandem fluorescent-tagged LC3. *Autophagy* **3**, 452–460 (2007).

Acknowledgments: We thank A. Díaz for help in the animal facility to grow and maintain our mouse cohorts and G. Herrera and B. Jávega Martínez for help in flow cytometry analysis, as well as all the technicians of the UCIM and SCSIE of the University of Valencia. We also thank S. Atencia for help in the muscle regeneration studies. **Funding:** This work was supported by the following grants: grants APOSTD/2018/230 from "Conselleria d'Educació, Investigació, Cultura i Esport," GV/2019/092 from "Conselleria d'Educació, Investigació, Cultura i Esport," and CIGE/2021/134 from "Conselleria d'Innovació, Universitats, Ciència y Societat Digital" to C.M.-B.; grant ACIF/2019/164 from "Conselleria d'Educació, Investigació, Cultura i Esport" to A.R.-D.; grants PID2020-113839RB-I00 funded by MCIN/AEI/10.13039/501100011033 and CIAICO/2022/190 funded by Conselleria de Educació, Universitats y Ocupació to C.B.; and CB16/10/00435 (CIBERFES) from Instituto de Salud Carlos III, PID2019-110906RB-I00/AEI/10.13039/501100011033 and RED2018-102576-T from the Spanish Ministry of Innovation and Science, PROMETEO/2019/097 from "Consellería de Educació de la Generalitat Valenciana," EU Funded H2020–DIABFRAILLATAM (ref. 825546), European Joint Programming Initiative "A Healthy Diet for a Healthy Life" (JPI HDHL), the ERA-NET Cofund ERA-HDHL (grant agreement no. 696295 of the EU Horizon 2020 Research and Innovation Programme), Fundación Ramón Areces, and Fundación Soria Melguizo to J.V. and National Institute on Aging (NIH) grant AG031782 to A.M.C. **Author contributions:** Conceptualization: C.M.-B., A.R.-D., N.R.-G., A.M.C.,

C.B., and J.V. Methodology: C.M.-B., A.R.-D., J.S.-R., N.R.-G., M.D., A.M.C., C.B., and J.V. Investigation: C.M.-B., A.R.-D., J.S.-R., N.R.-G., J.H.-A., and M.D. Visualization: C.M.-B., A.R.-D., C.B., and J.V. Supervision: A.M.C., C.B., and J.V. Writing—original draft: C.M.-B., A.R.-D., and J.V. Writing—review and editing: C.M.-B., A.M.C., C.B., and J.V. Resources: C.M.-B., A.R.-D., M.D., A.M.C., C.B., and J.V. Funding acquisition: C.M.-B., A.R.-D., A.M.C., C.B., and J.V. Data curation: C.M.-B. and A.R.-D. Validation: C.M.-B., A.R.-D., J.S.-R., M.D., C.B., and J.V. Formal analysis: C.M.-B., A.R.-D., J.S.-R., J.H.-A., and M.D. Software: C.M.-B. and A.R.-D. Project administration: A.R.-D., C.B., and J.V. **Competing interests:** A.M.C. is the founder and serves on the Scientific Board of Selphagy (a program under Life Biosciences). The other authors declare that they have no competing interests. **Data and materials availability:** All data needed to evaluate the conclusions in the paper are present in the paper and/or the Supplementary Materials.

Submitted 17 June 2024
Accepted 11 February 2025
Published 19 March 2025
10.1126/sciadv.adr1378